




Article

Chromium Isotope Systematics in Modern and Ancient Microbialites

Sylvie Bruggmann ^{1,2,*} , Alexandra S. Rodler ³, Robert M. Kläbe ⁴, Steven Goderis ³  and Robert Frei ¹ 

¹ Department of Geoscience and Natural Resource Management, Geology Section, University of Copenhagen, Øster Voldgade 10, K DK-1350 Copenhagen, Denmark; robertf@ign.ku.dk

² Department of Coastal and Marine Sciences, Rutgers University, 71 Dudley Rd, New Brunswick, NJ 08901, USA

³ Department of Chemistry, Analytical, Environmental and Geo-Chemistry Research Group, Vrije Universiteit Brussel, Pleinlaan 2, 1050 Brussels, Belgium; alexandra.rodler@vub.be (A.S.R.); steven.goderis@vub.be (S.G.)

⁴ Department of Earth Sciences, University of Adelaide, North Terrace, Adelaide, SA 5000, Australia; robert.klaebe@adelaide.edu.au

* Correspondence: bruggmann@marine.rutgers.edu

Received: 3 September 2020; Accepted: 18 October 2020; Published: 20 October 2020



Abstract: Changes in stable chromium isotopes (denoted as $\delta^{53}\text{Cr}$) in ancient carbonate sediments are increasingly used to reconstruct the oxygenation history in Earth's atmosphere and oceans through time. As a significant proportion of marine carbonate older than the Cambrian is microbially-mediated, the utility of $\delta^{53}\text{Cr}$ values in ancient carbonates hinges on whether these sediments accurately capture the isotope composition of their environment. We report Cr concentrations (Cr) and $\delta^{53}\text{Cr}$ values of modern marginal marine and non-marine microbial carbonates. These data are supported by stable C and O isotope compositions, as well as rare earth elements and yttrium (REY) concentrations. In addition, we present data on ancient analogs from Precambrian strata. Microbial carbonates from Marion Lake (Australia, $\delta^{53}\text{Cr} \approx 0.99\text{‰}$) and Mono Lake (USA, $\approx 0.78\text{‰}$) display significantly higher $\delta^{53}\text{Cr}$ values compared with ancient microbialites from the Andrée Land Group in Greenland (720 Ma, $\approx 0.36\text{‰}$) and the Bitter Springs Formation in Australia (800 Ma, $\approx -0.12\text{‰}$). The $\delta^{53}\text{Cr}$ values are homogenous within microbialite specimens and within individual study sites. This indicates that biological parameters, such as vital effects, causing highly variable $\delta^{53}\text{Cr}$ values in skeletal carbonates, do not induce variability in $\delta^{53}\text{Cr}$ values in microbialites. Together with stable C and O isotope compositions and REY patterns, $\delta^{53}\text{Cr}$ values in microbialites seem to be driven by environmental parameters such as background lithology and salinity. In support, our Cr and $\delta^{53}\text{Cr}$ results of ancient microbial carbonates agree well with data of abiotically precipitated carbonates of the Proterozoic. If detrital contamination is carefully assessed, microbialites have the potential to record the $\delta^{53}\text{Cr}$ values of the waters from which they precipitated. However, it remains unclear if these $\delta^{53}\text{Cr}$ values record (paleo-) redox conditions or rather result from other physico-chemical parameters.

Keywords: Cr isotopes; C isotopes; O isotopes; rare earth elements; Proterozoic; carbonates

1. Introduction

Sedimentary carbonates are increasingly examined for their chromium isotope composition ($\delta^{53}\text{Cr}$) to investigate the evolution of oxygen in the Earth's atmosphere and oceans (e.g., [1]). Chromium mobilization from igneous rocks is dependent on oxidative weathering (catalyzed by MnO_2), and thus, accumulation of Cr in marine sediments requires the presence of oxygen in the atmosphere (0.0003% to 0.003% of present atmospheric levels (PAL) [2]). Changes in the redox state

of Cr induce isotope fractionation, where the lighter Cr isotopes are preferred in reduction reactions, resulting in redox-dependent changes of $^{53}\text{Cr}/^{52}\text{Cr}$ [3–5]. The reduction of Cr associated with microbes also induces Cr isotope fractionation (e.g., [6,7]). In laboratory experiments, Cr is incorporated into the crystal lattice of calcite [8], which is expected to show marginal isotope fractionation in natural settings [8–10]. Despite the evidence of redox-dependent Cr isotope fractionation, a large range of fractionation effects can also occur without any involvement of redox changes but in the presence of ligands [11,12]. Modern biogenic carbonates show a wide range in $\delta^{53}\text{Cr}$ values and a negative offset relative to ambient seawater ($\Delta^{53}\text{Cr} \approx 0.0\text{‰}$ – 0.9‰) [13–19]. Despite the growing compilation of $\delta^{53}\text{Cr}$ values of modern carbonate materials, its large range in skeletal carbonates complicates their use as archives for paleo-reconstructions. A recent study presented promising Cr isotope data that were identical between microbial carbonate produced by red coralline algae and ambient seawater [17]. Still, data on Cr isotope systematics in modern non-skeletal carbonates [15] or carbonates in microbial mats remains scarce to date.

Microbial carbonate precipitation can be mediated by microbes directly or involves trapping and binding of sediment grains by biofilms [20–24]. The resulting organo-sedimentary carbonate structures (microbialites) are preserved in the rock record as early as 3.5 billion years ago (Ga) on the Pilbara Craton, Western Australia [25–28] or even as early as 3.7 Ga (Isua Greenstone Belt, Greenland [29]). In Precambrian strata, carbonate necessarily precipitated either microbially or abiotically since metazoan calcification had yet to evolve. Shallow rather than deeper water marine and continental carbonates are over-represented in the Precambrian record due to the lack of both oceanic crust and skeletal carbonate flux to the seafloor. Therefore, carbonate-based paleo-environmental studies rely heavily on shallow-water and typically microbially-mediated carbonates to reflect past seawater chemistry. However, the precise mechanisms driving microbialite formation and incorporation of trace metals are variable and difficult to determine in older carbonates, particularly where subsequent recrystallization during burial and diagenesis masks the texture and mineralogy of the initial precipitates. Yet, valuable paleo-environmental information may be preserved in cases where the local seawater chemistry is captured during carbonate precipitation.

Microbialites are known to grow under highly variable conditions, including extreme environments. Their adaptive capacity makes them invaluable archives to reconstruct such conditions in the past. However, the diverse microbial communities that are involved in forming microbialites may complicate the interpretation of geochemical data. Although poorly constrained, the metabolic activities of these communities may affect the incorporation of trace metals during carbonate formation, and thus not all microbialites may record environmental information.

Despite these uncertainties, microbial carbonates are extensively used as archives to reconstruct physico-chemical conditions of early Earth environments and to study the earliest forms of life [22,30,31], for example, by using variations in stable C and O isotopes as well as rare earth elements and yttrium (REY) patterns. Due to similar chemical properties of REY (e.g., uniform trivalent charge with the exception of Ce^{4+} and Eu^{2+}) and their similar size and charge, their reactions to chemical changes are similar and predictable [32,33]. Patterns of REY of (bio-) chemical sediments, including carbonates, in the geological record, were proposed to be capable of preserving the REY conditions of ambient seawater [31,32,34–36].

Here, we geochemically characterize modern microbialites from marginal marine and non-marine settings with the aim to evaluate systematics of Cr concentrations (Cr) and $\delta^{53}\text{Cr}$ values related to environmental and/or biological effects. We select two types of microbialites (tufa and stromatolites) from different environmental conditions. They serve as examples to test if they preserve the Cr isotope compositions of their environments, regardless of differences in their microbial community structure and composition. Thus, we aim at providing a first insight into the variability of Cr isotope data of different types of microbialites. Furthermore, we analyzed Cr and $\delta^{53}\text{Cr}$ values of Proterozoic microbialites to explore the microbialite-Cr-isotope record for paleo-environments. The (paleo-)

environmental context is also characterized by stable O ($\delta^{18}\text{O}$) and C ($\delta^{13}\text{C}$) isotope data as well as REY patterns.

2. Materials and Methods

The microbialites investigated in this study (Table 1, Figure 1) are mainly laminated microbialites (stromatolites) or tufa, the latter of which precipitate due to the influx of Ca-rich submerged springs into an alkaline freshwater lake (Mono Lake) [30,37]. We investigated microbialite samples from two different modern microbial carbonate-producing locations, the coastal Marion Lake, and the inland Mono Lake (Figure 2). The modern microbialites (Marion Lake, Mono Lake) were provided by the University of Adelaide, Australia (Table 1). Further, we analyzed microbialite samples from two Precambrian carbonate-dominated sections from a marine (Andrée Land Group (ALG), Greenland, ~720 Ma; [38]) and non-marine setting (Bitter Springs Formation (BSF), Australia, ~800 Ma; [39]).

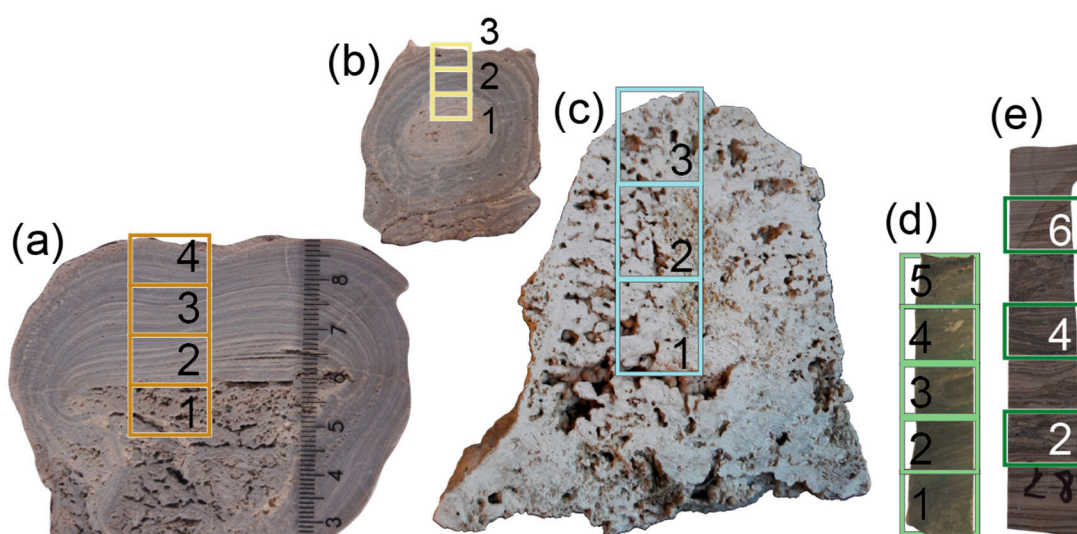


Figure 1. Photographs of microbialite samples, numbered boxes indicating sample positions (cm-scale in (a) applies for all samples, see also Table 1). Two specimens from Marion Lake (MRN) were investigated: (a) profile A, (b) profile B. (c) Mono Lake, (d) Andrée Land Group (ALG; bulk sample not indicated), (e) Bitter Springs Formation (BSF).

Table 1. Description of microbialite samples. Positions represent inner to outer parts of the microbialite samples (see Figure 1). For water sample sites and geological background, see Figure 2.

Sample ID	Location	Sample Type	Position	Sample Characterization	Age
MRN-A-1	Marion Lake, Australia	carbonate profile A	1	Fine-grained, thinly laminated microbialites formed in a hypersaline lake with marine connection	Recent
MRN-A-2		carbonate profile A	2		
MRN-A-3		carbonate profile A	3		
MRN-A-4		carbonate profile A	4		
MRN-B-1		carbonate profile B	1		
MRN-B-2		carbonate profile B	2		
MRN-B-3		carbonate profile B	3		
Mono-1	Mono Lake, USA	carbonate profile	1	Tufa formed in an inland, alkaline freshwater lake	Recent
Mono-2		carbonate profile	2		
Mono-3		carbonate profile	3		
ALG-B	Andrée Land Group, Greenland	carbonate bulk	7	Dolomitized stromatolites formed on a carbonate ramp in a marine environment	≈720 Ma
ALG-1		carbonate profile	1		
ALG-2		carbonate profile	2		
ALG-3		carbonate profile	3		
ALG-4		carbonate profile	4		
ALG-5		carbonate profile	5		
BSF-2	Bitter Springs Formation, Australia	carbonate profile	2	Cyclic stromatolitic carbonates formed under restricted marine to alkaline lacustrine conditions	≈800 Ma
BSF-4		carbonate profile	4		
BSF-6		carbonate profile	6		

MRN = Marion Lake, Mono = Mono Lake, ALG = Andrée Land Group, and BSF = Bitter Springs Formation.

2.1. Sample Description

Marion Lake is part of a lagoon system situated in a depression on the Yorke Peninsula in South Australia (Australia; Figure 2). Due to late Pleistocene and Holocene transgressions, the depression was flooded multiple times and turned into a shallow strait. Protected by accreted coastal barriers, a marine unit of fossiliferous seagrass carbonate accumulated [40]. Subsequently, the environment evolved into a shallow lake system where gypsum deposited [40]. A proportion of the seagrass carbonate is underlying a unit of porous limestone (boxwork limestone) capped by a thin (10 cm) stromatolitic limestone (3780 ± 110 years) [41]. This stromatolitic limestone contains finely laminated undulatory stromatolites, such as the samples investigated in this study. Today, Marion Lake is a hypersaline [42] gypsum-carbonate lake on a regressive marginal flat with a connection to open marine conditions [43] and a pH of between 7.4 and 7.9 (measured in this study). Within this marginal flat, fine-grained, thinly laminated microbialites form [24,40]. They constitute low-Mg calcite and aragonite with well-preserved relics of microfossils (bacteria) and extracellular polymeric substances (EPS), and generally lack detrital material [24,40]. The lack of detrital particles and the thin micritic laminae with microfossils indicate that these carbonate precipitates were mediated by microbes [24].

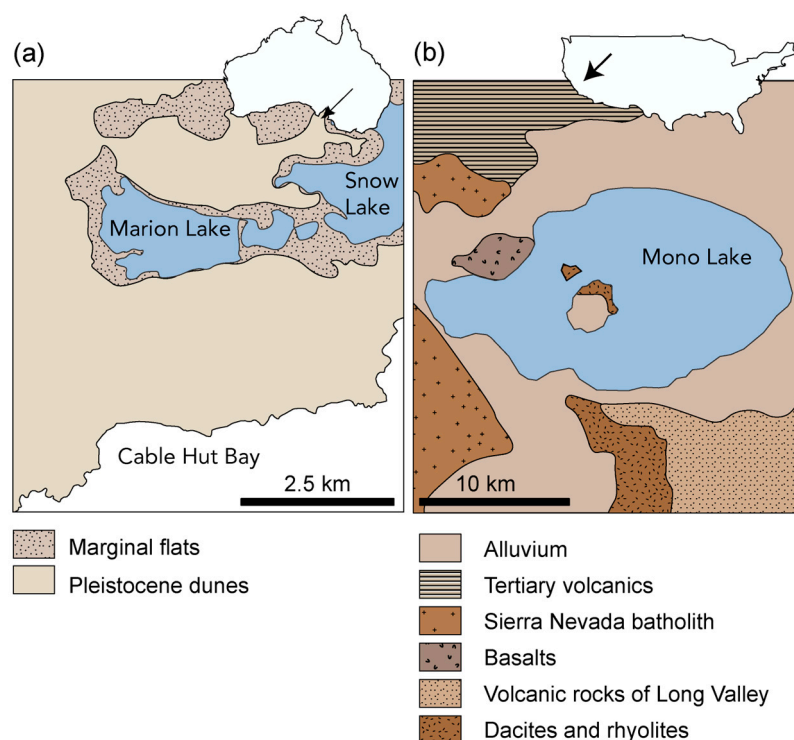


Figure 2. Maps of (a) Marion Lake (Yorke Peninsula in South Australia, Australia) and (b) Mono Lake (CA, USA) indicating the geological background. The maps are modified after [24,44].

Mono Lake is located in Central California on the eastern slope of the Sierra Nevada mountain range (USA, Figure 2). Mono Lake is located in a structural basin and surrounded by mainly Cenozoic volcanic rocks [44]. The water level of Mono Lake has been affected severely by anthropogenic influence, as inflow streams were diverted to the Los Angeles Aqueduct [44]. This induced a drop in the water level of more than 12 m, as well as increased concentrations of solutes in the remaining water. Facilitated by the low water level, the annual mixing during winter has occasionally been interrupted (e.g., induced by heavy rainfalls) and lead to meromixis (e.g., [45]). Today, Mono Lake is a closed basin lake with hypersaline conditions (90 g/L), high alkalinity ($\text{pH} \geq 9.2$), and high dissolved organic carbon ($\text{DOC} \approx 6.7 \text{ mM}$) surrounded [44–47]. Freshwater influx is delivered by streams, groundwater as well as hot springs [44,48]. Bicarbonate-rich lake water mixes with a Ca-rich groundwater influx,

calcite tufa precipitate mediated by microbial activity (Figure 1) [37,49–51]. The precise age of the sample is unknown.

The Andrée Land Group (ALG; NE Greenland) formed approximately 720 Ma on a carbonate ramp [38]. Selected dolomitized stromatolites from ALG serve as ancient marine analogs of microbialites. The well-preserved stromatolites from the Bitter Springs Formation (BSF; Loves Creek, Australia, ~800 Ma; Figure 1) belong to a unit of cyclic stromatolitic carbonates. The environmental conditions of the BSF (recently also referred to as Bitter Springs Group) changed from restricted marine to alkaline lacustrine. Our samples belonged to the Johnny Creek Formation and were deposited under non-marine evaporative conditions [39].

2.2. Sample Preparation

The microbialites were cut in approximately 1 cm³ cubes along profiles perpendicular to the lamination or along a core to rim profile (indicated in Figure 1) to capture overall internal variations. For ALG, a larger sample (~15 cm³) was additionally analyzed and is referred to as “bulk” (ALG-B; Table 1). Microbialite samples were powdered and dissolved in 0.5 mol/L HCl, and aliquots of the dissolved samples were analyzed for major, trace, and REY concentrations as well as Cr isotope ratios. Powders of microbialite samples were additionally analyzed for their $\delta^{18}\text{O}$ and $\delta^{13}\text{C}$ values.

2.3. Chromium Isotope Analysis

Powdered microbialite samples containing approximately 300 ng Cr were dissolved in 0.5 mol/L HCl, centrifuged, and the supernatant was collected and filtered through 0.45 μm nylon membrane filters (Advantec MFS) before ion chromatography. The microbialite samples were spiked with an adequate amount of ^{50}Cr – ^{54}Cr double spike and evaporated to dryness [3,52,53]. Samples were then re-dissolved in aqua regia to ensure equilibration between sample and spike and dried down again. To separate Cr from microbialite samples, chromatographic Cr separation modified after [54–56] was applied. In short, microbialite samples were re-dissolved with 20 mL of a 0.025 mol/L HCl solution containing 0.5 mL of 0.2 mol/L $(\text{NH}_4)_2\text{S}_2\text{O}_8$, capped, and boiled for 1 h to oxidize Cr(III) to Cr(VI). After cooling to room temperature, the samples were subject to an anion column containing pre-cleaned Dowex AG 1 \times 8 anion resin. Next, the resin was rinsed with 10 mL 0.2 mol/L HCl, 2 mL 2 mol/L HCl and 5 mL Milli-QTM water (18.2 M Ω cm, hereafter MQ). Chromium was then reduced and eluted with 2 mol/L HNO_3 and 5% H_2O_2 . The eluent was evaporated to dryness, re-dissolved in 100 μL concentrated double-distilled HCl on a hotplate for 10 min, and subsequently diluted with 2.3 mL MQ. These solutions were then passed over a pre-cleaned Dowex AG50W-X8 (200–400 mesh) cation exchange resin, and the final eluents were immediately collected in SavillexTM Teflon beakers. Another 8 mL of 0.5 mol/L HCl was used to collect the remaining Cr. The final Cr sample was evaporated to dryness; matrix elements (for example, Mn, Mg, Ca, or Al) were retained in the resin during ion chromatography.

The final Cr samples were loaded onto outgassed Re filaments using 2 μL of a 2:1:0.5 mixture of silica gel, 0.5 mol/L H_3PO_4 and 0.5 mol/L H_3BO_3 . Both Cr concentrations and isotope ratios were analyzed using an IsotopX/GV IsoProbe T thermal ionization mass spectrometer (TIMS) equipped with eight Faraday cups at the University of Copenhagen, Denmark. Four Cr beams ($^{50}\text{Cr}^+$, $^{52}\text{Cr}^+$, $^{53}\text{Cr}^+$, and $^{54}\text{Cr}^+$) were analyzed simultaneously with $^{49}\text{Ti}^+$, $^{51}\text{V}^+$, and $^{56}\text{Fe}^+$ beams, which were used to monitor interfering ions. Each sample was analyzed at approximately 1100 $^\circ\text{C}$ with a ^{52}Cr ion beam of between 350 and 1000 mV in 1 to 3 runs per loaded sample. Each run consisted of 120 cycles grouped into 24 blocks (5 cycles each) with 10 s integration periods and 20 s baseline measurements at ± 0.5 AMU. The raw data were corrected for naturally- and instrumentally-induced isotope fractionation using the double spike routine of [53]. The corrected values are reported in delta notation (‰) with 2SD (Table 2; Equation (1)).

$$\delta^{53}\text{Cr} = \left(\frac{(^{53}\text{Cr}/^{52}\text{Cr})_{\text{sample}}}{(^{53}\text{Cr}/^{52}\text{Cr})_{\text{NIST SRM979}}} - 1 \right) \times 1000 \quad (1)$$

Table 2. Chromium concentrations (ppm for solids, in nM for liquids) and stable Cr, C, and O isotope data.

Sample ID	Cr	$\delta^{53}\text{Cr}$	2SD	$\delta^{13}\text{C}$	SD	$\delta^{18}\text{O}$	SD
	ppm (nM)	‰		‰		‰	
MRN-A-1	6.06	0.99	0.02	2.61	0.05	0.71	0.06
MRN-A-2	3.09	0.94	0.00	1.97	0.10	1.73	0.17
MRN-A-3	1.68	1.01	0.05	2.74	0.08	0.75	0.10
MRN-A-4	1.68	0.93	0.05	2.58	0.07	0.59	0.14
MRN-B-1	1.78	0.94	0.02	2.78	0.08	0.46	0.07
MRN-B-2	1.89	1.07	0.10	2.85	0.08	0.77	0.17
MRN-B-3	1.50	1.03	0.04	2.66	0.09	0.27	0.12
Mono-1	0.74	0.85	0.14	8.14	0.08	−2.47	0.14
Mono-2	0.69	0.79	0.02	8.43	0.05	−2.08	0.11
Mono-3	0.86	0.71	0.00	8.52	0.11	−1.50	0.11
ALG-B	2.85	0.33	0.08	4.27	0.09	−3.54	0.18
ALG-1	1.67	0.37	0.02	3.73	0.13	−2.63	0.15
ALG-2	3.21	0.43	0.05	3.79	0.13	−3.06	0.20
ALG-3	3.30	0.42	0.05	3.81	0.14	−3.24	0.17
ALG-4	4.24	0.36	0.08	3.70	0.14	−3.07	0.19
ALG-5	4.57	0.23	0.07	3.80	0.11	−3.78	0.17
BSF-1	2.38	−0.14	0.02	−0.48	0.15	−6.53	0.21
BSF-2	2.23	−0.18	0.06	−0.35	0.03	−7.09	0.08
BSF-3	2.18	−0.04	0.07	−0.31	0.06	−6.91	0.12

To assess the precision of our analyses, a double-spike treated, certified standard reference material (NIST SRM 979) was analyzed two to three times, which resulted in an external reproducibility of $0.00 \pm 0.13\text{‰}$ and $0.05 \pm 0.09\text{‰}$ (2SD) for ^{52}Cr ion beam intensities of 500 mV and 1000 mV, respectively. Repeated analyses of certified carbonate standards (JDo-1, JLS-1) resulted in Cr and $\delta^{53}\text{Cr}$ values within the range of published values [9,14,57,58]. Procedural blanks consistently resulted in Cr of <8 ng for water samples and ≈ 1 ng for microbialite samples.

The $\delta^{53}\text{Cr}$ values of sediment samples can be corrected for detrital contamination using concentrations of Al or Ti as immobile reference elements as outlined by [54,56,59]. Briefly, detrital Cr (Cr_{det}) is calculated as $\text{Cr}_{\text{det}} = \text{Al}_{\text{sample}}/\text{Al}_{\text{det}} \times \text{Cr}_{\text{det}}$. We applied a detrital correction (Equations (2) and (3)) to the results of the microbialite samples using the crustal Cr/Al ratio ($(\text{Cr}/\text{Al})_{\text{det}}$) of [60] together with the $\delta^{53}\text{Cr}$ value of the average crust ($\delta^{53}\text{Cr}_{\text{det}} = -0.12 \pm 0.10\text{‰}$, 2SE; [53]).

$$\delta^{53}\text{Cr}_{\text{auth}} = \frac{\delta^{53}\text{Cr} - \delta^{53}\text{Cr}_{\text{det}} \times f_{\text{det}}}{1 - f_{\text{det}}} \quad (2)$$

The fraction of detritally contributed Cr (f_{det}) is defined according to Equation (3).

$$f_{\text{det}} = \frac{\text{Al}_{\text{sample}} \times \left(\frac{\text{Cr}}{\text{Al}}\right)_{\text{det}}}{\text{Cr}_{\text{sample}}} \quad (3)$$

2.4. Stable O and C Isotope Analysis

Aliquots of the powdered microbialite samples (0.6–1.0 mg) were placed into 3.5 mL glass vials, sealed with rubber septa, flushed with He and allowed to react with in excess 104% phosphoric acid (H_3PO_4) at 70 °C. After a reaction time of 100 min, they were routinely analysed for their stable C and O isotope values at the Analytical, Environmental and Geo-Chemistry lab at the Vrije Universiteit Brussel, Belgium, using a Nu Perspective isotope ratio mass spectrometry (IRMS) coupled with an automatic gas sampling system (GasPrep from Nu Instruments). The stable C and O isotope values are reported as $\delta^{13}\text{C}$ and $\delta^{18}\text{O}$, respectively, and given in permille relative to the Vienna Pee Dee Belemnite

standard (‰ VPDB). The reproducibility of replicated standard materials is based on analyses of the certified reference materials IAEA 603 and IAEA CO-8 along with an in-house standard (MAR-2(3)), and is better than 0.12‰ and 0.21‰ for C and O isotope values (2σ , $n = 48$), respectively. All samples were analysed three times; these repeat analyses were used for calculating average values and standard deviation (1SD).

2.5. Elemental Concentrations and REY

Aliquots of the dissolved microbialite samples were analysed for major, trace and REY patterns with inductively coupled plasma mass spectrometry (ICP-MS; Bruker Daltonics Aurora Elite) at the University of Copenhagen. The sample aliquots along with certified standard reference materials (limestone: JLS-1; basalt: BHVO-1) were diluted in 2% HNO₃ and analysed along with calibration solutions. The concentrations of REY were normalised (S_N) to the Post Archean Australian Shale (PAAS; [61]). Anomalies of Y, Eu and Ce were calculated using Y/Ho_{SN} , $Eu_{SN}/Eu^*_{SN} = Eu_{SN} / (0.67 \times Sm_{SN} + 0.33 \times Tb_{SN})$ and $Ce_{SN}/Ce^*_{SN} = Ce_{SN} / (2 \times Pr_{SN} - Nd_{SN})$, respectively [62–65]. Following [66], La concentrations were not used in the calculations as La anomalies caused by e.g., high salinity, can affect Ce_{SN}/Ce^*_{SN} . The light REY_{SN} (LREE) include the elements La to Eu, the heavy REY_{SN} (HREE) comprise Gd to Lu.

3. Results

3.1. Chromium Concentrations and Isotope Compositions

The microbialite samples show Cr between 0.69 to 1.89 ppm in the case of modern samples, with two outliers of 3.09 and 6.09 ppm (MRN), and between 1.67 and 4.57 ppm for Precambrian samples (Figure 3). The Cr in the microbialite samples were too low for sub-millimetric Cr isotope analysis and/or the microbialite laminae were too thin to be sampled individually, and thus, multiple laminae were sampled at a time.

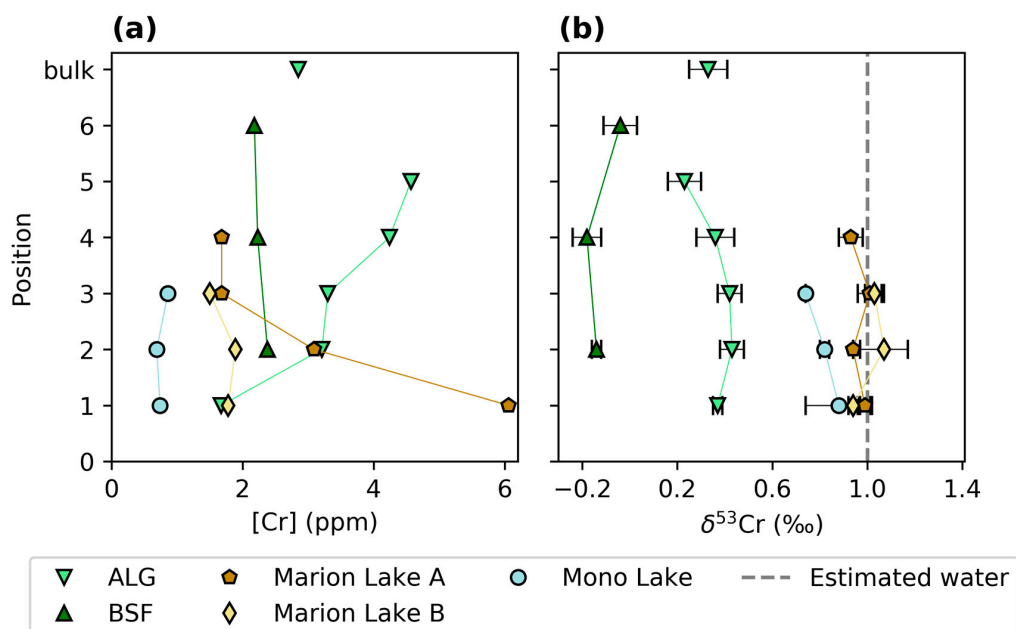


Figure 3. Cr concentrations (a) and isotope compositions (b) of microbialites and the estimated Marion Lake water samples (dashed grey line). Numbers on y-axis indicate the sample position (see Figure 1 and Table 1).

The $\delta^{53}\text{Cr}$ values of all modern microbialite samples lie within a narrow range of 0.71 to 1.07‰, with $\delta^{53}\text{Cr}$ variations from $0.93 \pm 0.05\text{‰}$ (2SD) to $1.07 \pm 0.10\text{‰}$ for Marion Lake and from $0.71 \pm 0.05\text{‰}$ to $0.85 \pm 0.14\text{‰}$ for Mono Lake (Table 2). Ancient microbialites in this study displayed Cr isotope ranges from $0.23 \pm 0.07\text{‰}$ to $0.43 \pm 0.05\text{‰}$ and from $-0.18 \pm 0.06\text{‰}$ to $-0.14 \pm 0.02\text{‰}$, for ALG and BSF, respectively (Table 2). The samples from Mono Lake and BSF showed low Cr/Al ratios in a range similar to or higher than the reference material and are thus unsuitable for detrital correction. In contrast, detrital Cr only contributed 5 to 24% to most samples from Marion Lake and ALG samples and was thus suitable for detrital correction (Figure 4; Table 3) [54,67]. However, the detritus-corrected $\delta^{53}\text{Cr}$ values for Marion Lake and ALG samples were within the error of or only slightly higher than the uncorrected $\delta^{53}\text{Cr}$ values (Table 3). Thus, we refer to uncorrected $\delta^{53}\text{Cr}$ values for all samples throughout the manuscript.

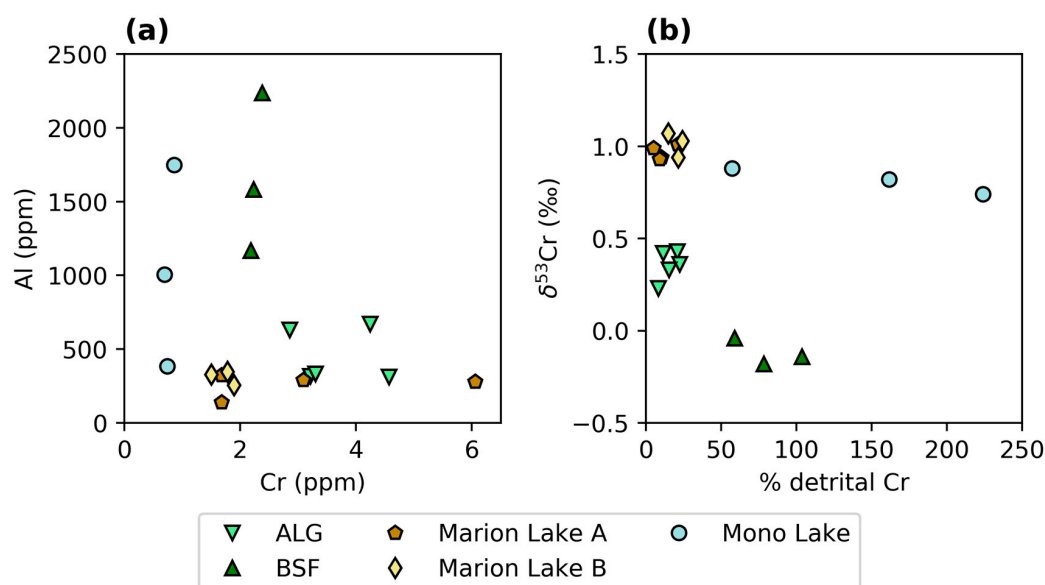


Figure 4. Cross-plot of (a) Cr and Al concentrations and (b) % of detrital Cr and (uncorrected) $\delta^{53}\text{Cr}$ values.

Table 3. Calculations for detrital correction of $\delta^{53}\text{Cr}$ values using Al concentrations.

Sample ID	Cr	Al	Cr/Al $\times 1000$	Cr _{det}	Cr _{auth}	Cr _{det}	f	$\delta^{53}\text{Cr}$	$\delta^{53}\text{Cr}_{\text{auth}}$
	ppm	ppm		ppm	ppm	%		‰	‰
MRN-A-1	6.06	280	22	0.31	5.75	5.08	0.05	0.99	0.99
MRN-A-2	3.09	290	11	0.32	2.77	10.3	0.10	0.94	0.95
MRN-A-3	1.68	324	5	0.36	1.32	21.3	0.21	1.01	1.09
MRN-A-4	1.68	139	12	0.15	1.52	9.14	0.09	0.93	0.94
MRN-B-1	1.78	347	5	0.38	1.40	21.5	0.21	0.94	1.02
MRN-B-2	1.89	256	7	0.28	1.61	14.9	0.15	1.07	1.11
MRN-B-3	1.50	329	5	0.36	1.13	24.2	0.24	1.03	1.15
Mono-1	0.74	383	2	0.42	0.31	57.3	0.57	0.85	2.61
Mono-2	0.69	1006	1	1.11	-0.42	162	1.61	0.79	7.12
Mono-3	0.86	1748	0	1.92	-1.06	224	2.24	0.71	3.44
ALG-1	1.67	317	5	0.35	1.32	20.8	0.21	0.37	0.40
ALG-2	3.21	332	10	0.37	2.85	11.4	0.11	0.43	0.44
ALG-3	3.30	672	5	0.74	2.56	22.4	0.22	0.42	0.47
ALG-4	4.24	313	14	0.34	3.89	8.13	0.08	0.36	0.36
ALG-5	4.57	632	7	0.70	3.88	15.2	0.15	0.23	0.24
BSF-1	2.38	2238	1	2.46	-0.09	104	1.04	-0.14	-14.29
BSF-2	2.23	1582	1	1.74	0.49	78.2	0.78	-0.18	-0.87
BSF-3	2.18	1168	2	1.28	0.90	58.8	0.59	-0.04	0.13

3.2. Stable O and C Isotopes

Both Lake Marion and Mono Lake microbialites displayed high $\delta^{13}\text{C}$ values of between +1.97–+8.52‰ (Figure 5; Table 2). Oxygen isotope values of Lake Marion carbonate samples are +0.46–+1.73‰, which are high compared with Mono Lake samples with $\delta^{18}\text{O}$ values of −2.47–−1.50‰.

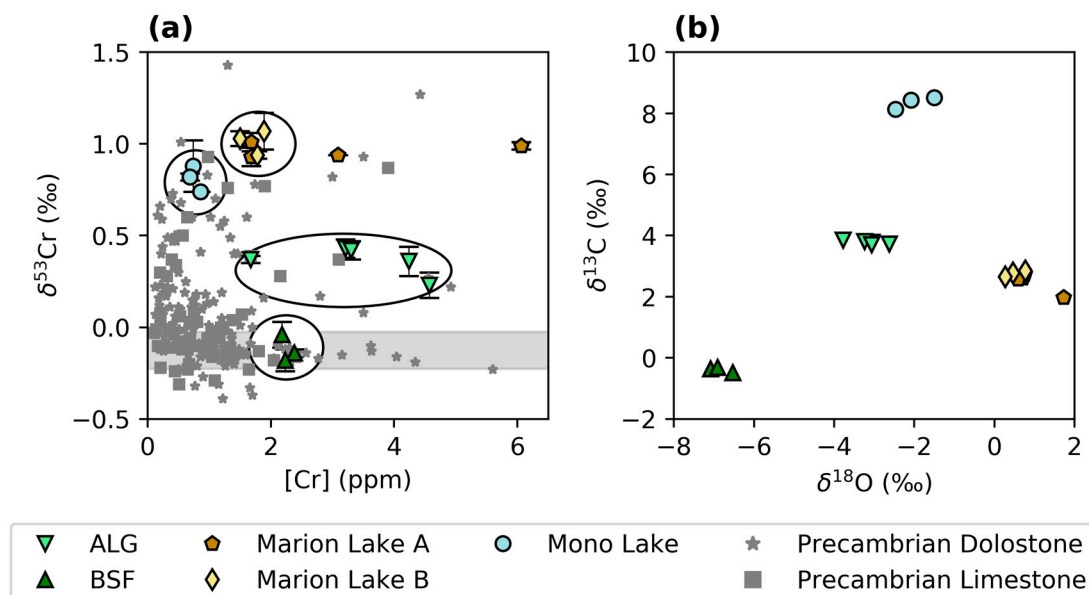


Figure 5. (a) Cr as a function of $\delta^{53}\text{Cr}$ values with circles highlighting site-specific $\delta^{53}\text{Cr}$ values, and grey horizontal area representing $\delta^{53}\text{Cr}$ values of detrital material [53]. Literature values of dolostones and limestones from the Precambrian are published in [67–69]. (b) Stable C and O isotope ratios, illustrating the differences in the depositional environments and/or the degree of diagenetic overprinting.

The Precambrian microbialites had relatively low $\delta^{18}\text{O}$ values compared with their modern counterparts. The ALG samples were only slightly lower (approximately $-3.20 \pm 0.37\text{‰}$, 2SD) than those from Mono Lake, while the BSF samples had the lowest $\delta^{18}\text{O}$ values (approximately $-6.84 \pm 0.29\text{‰}$) of all microbialites analysed in this work. Furthermore, BSF samples had low $\delta^{13}\text{C}$ values in a narrow range of -0.31 ± 0.07 to $-0.48 \pm 0.16\text{‰}$ (SD), while ALG samples had high $\delta^{13}\text{C}$ values ($+3.85 \pm 0.21\text{‰}$, 2SD) in a similar range as Marion Lake samples.

3.3. Elemental Concentrations and REY

The concentrations of specific trace (Cr) and REY elements are listed in Tables 2 and 4, respectively. Patterns of REY are normalised to a standard reference material (Post Archean Australian Shale; [61]. The REY patterns of Marion Lake microbialites co-varied with seawater REY patterns with a near-shore depositional setting (negative Ce anomaly, positive Y anomaly, $\text{Y}/\text{Ho}_{\text{SN}} \approx 48$, enrichment in heavy REY; [32,70]) (Figure 6; Table 4). Mono Lake samples deviated from the REY pattern of the basalt standard, showing a positive Ce anomaly and a slight increase in the HREE.

Table 4. Calculated REY ratios for samples and standards.

Sample ID	La	Ce	Pr	Nd	Sm	Eu	Gd	Tb	Dy	Y	Ho	Er	Tm	Yb	Lu	Nd _{SN} / Yb _{SN}	Y/Ho	Y _{SN} / Ho _{SN}	Er _{SN} / Yb _{SN}	Yb _{SN} / Pr _{SN}	Ce _{SN} / Ce* _{SN}	Eu _{SN} / Eu* _{SN}
BHVO-2 ¹	0.72	0.83	1.09	1.41	1.96	3.67	2.44	2.55	2.27	1.56	1.96	1.69	1.36	1.37	1.18	1.03	22.32	0.80	1.24	1.25	1.07	1.71
JDo-1 ²	0.21	0.03	0.12	0.14	0.14	0.16	0.22	0.18	0.19	0.39	0.18	0.18	0.12	0.12	0.09	1.19	59.62	2.13	1.49	1.03	0.30	1.06
MRN-A-1	0.03	0.01	0.02	0.03	0.03	0.05	0.05	0.04	0.05	0.08	0.04	0.05	0.03	0.04	0.03	0.81	49.30	1.76	1.23	1.55	0.48	1.32
MRN-A-2	0.04	0.01	0.03	0.04	0.04	0.06	0.06	0.05	0.05	0.09	0.05	0.05	0.04	0.04	0.04	0.99	48.94	1.75	1.27	1.25	0.37	1.24
MRN-A-3	0.04	0.01	0.04	0.05	0.05	0.07	0.07	0.06	0.07	0.11	0.07	0.07	0.05	0.05	0.05	0.88	46.16	1.65	1.29	1.40	0.49	1.21
MRN-A-4	0.03	0.01	0.03	0.04	0.04	0.06	0.06	0.05	0.06	0.09	0.06	0.06	0.04	0.04	0.04	0.84	47.47	1.70	1.33	1.48	0.45	1.22
MRN-B-1	0.03	0.01	0.03	0.04	0.05	0.06	0.06	0.06	0.07	0.11	0.06	0.07	0.05	0.06	0.05	0.70	47.13	1.68	1.26	1.84	0.68	1.21
MRN-B-2	0.03	0.01	0.03	0.04	0.05	0.07	0.07	0.07	0.08	0.12	0.08	0.08	0.06	0.06	0.05	0.72	45.89	1.64	1.31	1.81	0.61	1.26
MRN-B-3	0.02	0.01	0.02	0.03	0.04	0.05	0.05	0.05	0.06	0.10	0.06	0.06	0.05	0.05	0.05	0.57	49.23	1.76	1.16	2.25	0.69	1.23
Mono-1	0.30	0.41	0.35	0.40	0.48	1.07	0.58	0.57	0.62	0.59	0.57	0.64	0.54	0.72	0.64	0.56	29.02	1.04	0.88	2.07	1.40	2.11
Mono-2	0.30	0.51	0.42	0.50	0.71	1.28	0.90	0.99	1.16	1.08	1.08	1.21	1.09	1.48	1.30	0.34	28.11	1.00	0.82	3.54	1.54	1.59
Mono-3	0.27	0.43	0.34	0.41	0.55	1.10	0.72	0.77	0.89	0.87	0.84	0.94	0.81	1.06	0.91	0.39	28.95	1.03	0.89	3.11	1.57	1.76
ALG-1	0.13	0.15	0.15	0.16	0.19	0.28	0.23	0.19	0.18	0.16	0.15	0.15	0.11	0.13	0.10	1.28	29.76	1.06	1.17	0.89	1.22	1.50
ALG-2	0.10	0.12	0.12	0.13	0.15	0.15	0.17	0.15	0.15	0.12	0.12	0.12	0.09	0.10	0.08	1.31	29.57	1.06	1.17	0.85	1.14	1.03
ALG-3	0.08	0.09	0.09	0.10	0.11	0.12	0.13	0.11	0.11	0.09	0.09	0.09	0.07	0.08	0.06	1.29	29.75	1.06	1.17	0.87	1.17	1.07
ALG-4	0.07	0.09	0.10	0.12	0.12	0.13	0.14	0.11	0.10	0.08	0.08	0.07	0.05	0.06	0.05	1.96	30.18	1.08	1.26	0.60	1.09	1.06
ALG-5	0.07	0.08	0.10	0.11	0.12	0.12	0.13	0.11	0.09	0.07	0.07	0.07	0.05	0.05	0.04	2.21	29.59	1.06	1.31	0.53	1.05	1.02
BSF-1	0.17	0.23	0.26	0.31	0.33	0.32	0.37	0.29	0.26	0.21	0.20	0.19	0.13	0.15	0.12	2.03	29.84	1.07	1.25	0.59	1.09	1.01
BSF-2	0.09	0.11	0.13	0.15	0.15	0.14	0.17	0.13	0.11	0.09	0.08	0.08	0.05	0.06	0.05	2.54	30.73	1.10	1.33	0.45	1.05	1.02
BSF-3	0.11	0.15	0.16	0.19	0.21	0.20	0.23	0.18	0.16	0.13	0.12	0.12	0.08	0.10	0.07	2.04	30.57	1.09	1.25	0.58	1.08	1.02

¹ BHVO-2 = basalt standard, $n = 2$; ² JDo-1 = Dolostone standard, $n = 3$; SN = normalised to the Post Archean Australian Shale (PAAS), REY = rare earth elements and yttrium.

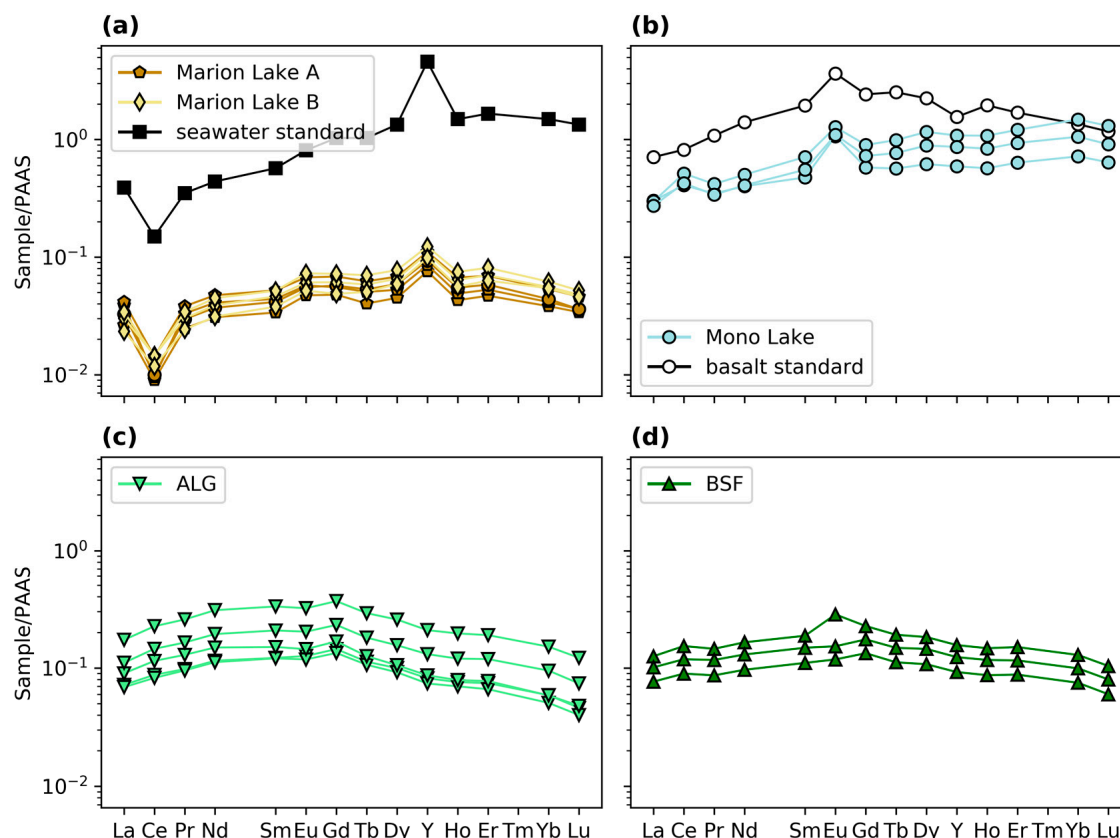


Figure 6. REY patterns of microbialites from (a) Marion Lake with REY distribution of a seawater standard [71], (b) Mono Lake with a basalt standard (BHVO-2), and ancient microbialites from (c) Andr  e Land Group (ALG) and (d) Bitter Springs Formation.

The REY patterns of the ancient microbialite samples (BSF and ALG) showed less distinct REY patterns and are rather flat (Figure 6; Table 4). They differed from typical seawater patterns, containing depleted HREE and no Y anomaly. The slight convexity of REY patterns with peak concentrations of Gd in ALG microbialites closely resembled REY patterns of shallow marine conditions [72], which are in line with the depositional environment of a carbonate ramp in a rift basin. The REY patterns of BSF showed a similar convexity as ALG, and the positive Eu resembled the basalt standard (indicated in Figure 6).

4. Discussion

4.1. Modern Microbialites

4.1.1. Geochemistry of Modern Microbialites

Due to their abundance in Precambrian strata, microbial carbonates have the potential to record past seawater chemistry. We present the first Cr isotope data of modern microbialites and found homogeneous Cr and $\delta^{53}\text{Cr}$ values in our samples. In both studied locations, $\delta^{53}\text{Cr}$ values displayed a tight range (Marion Lake: $0.99 \pm 0.11\text{‰}$; Mono Lake: $0.78 \pm 0.14\text{‰}$; Figure 3). Apart from two Cr outliers in the nucleus of the Marion Lake microbialites, we did not observe significant internal variation in Cr or $\delta^{53}\text{Cr}$ values ($2\text{SD} \leq 0.14\text{‰}$ per transect; $n = 3$ and 4 , respectively; Figure 3). The outliers in Cr (Marion Lake, position 1:6.06 ppm and the adjacent sample, position 2:3.09 ppm) were sampled from and close to the nucleus of the microbialite, where Cr may have accumulated more efficiently compared with the laminae. This might be because the microbial mat started to grow around a nucleus

consisting of a piece of carbonate, which perhaps originates from a different depositional and temporal setting. Despite Cr outliers in the nucleus of the Marion Lake microbialites, $\delta^{53}\text{Cr}$ values are consistent across laminae (0.93–1.07‰; Figure 3).

Multiple laminae were combined in individual samples, which may have homogenised sub-millimetric heterogeneity. Thus, Cr in our samples seemed homogeneous, at least on the scale sampled here. Trace elements, such as Fe, Cu, Zn, and As, are known to be heterogeneously distributed between laminae, and this can also be the case for Cr [73,74]. These elements are enriched on a sub-millimetric scale in certain laminae or mineral phases. The enrichment was attributed to passive binding of cations to EPS in the surface of a microbial mat and re-distribution into sulfide-rich laminae upon degradation of EPS during early diagenesis [73,74]. Thus, Cr is likely to show similar small-scale variations. While the methods applied in this study cannot resolve Cr variations in individual laminae, the tight ranges in Cr and $\delta^{53}\text{Cr}$ values measured suggest that intra-lamina variation is minimal. Here, we focused on capturing overall internal variations since we aim to create a framework to reconstruct long-term biogeochemical changes. Similarly to the homogeneous Cr distribution, $\delta^{13}\text{C}$ and $\delta^{18}\text{O}$ values of our modern samples fell into a tight range at both locations (Figure 5). The homogeneity of these geochemical tools across laminae suggests that these microbialites record relatively stable water column Cr, $\delta^{53}\text{Cr}$ as well as $\delta^{13}\text{C}$ and $\delta^{18}\text{O}$ values.

The contribution of detrital material in Mono Lake microbialites (>57% detrital Cr) was significantly higher than the fractions of <24% determined for Marion Lake samples. This coincided with the $\delta^{53}\text{Cr}$ values of Mono Lake microbialites ($\approx 0.78\text{‰}$), which were slightly lower than those of Marion Lake samples ($\approx 0.99\text{‰}$). The calculated high detrital Cr contributions were indicative of the influence of weathering of igneous rocks nearby Mono Lake, presumably carrying a typical detrital $\delta^{53}\text{Cr}$ value of -0.12‰ . The $\delta^{53}\text{Cr}$ values of Mono Lake microbialites were well above the detrital $\delta^{53}\text{Cr}$ value. Still, we suggest that detrital material can have a significant impact on $\delta^{53}\text{Cr}$ values in samples with high detrital Cr. Especially in samples that were deposited in environments with igneous or Al-rich lithologies and thus high background levels of Cr, detrital contamination should be carefully assessed, even if their Cr isotope compositions are above typical detrital $\delta^{53}\text{Cr}$ values.

4.1.2. Biological Controls on $\delta^{53}\text{Cr}$ Values in Modern Microbialites

The homogeneous Cr distribution and $\delta^{53}\text{Cr}$ values we observed in our microbialites contrast the heterogeneous Cr distribution and highly variable $\delta^{53}\text{Cr}$ values measured in modern skeletal carbonates (e.g., [13–19,75]). Although the impact of vital effects on $\delta^{53}\text{Cr}$ values is poorly constrained, some of these studies suggest that the large variability in $\delta^{53}\text{Cr}$ values within a single or between several specimen(s) of metazoan species can be caused by vital effects. Microbial carbonate precipitation does not involve higher organisms and thus, the variability in $\delta^{53}\text{Cr}$ values in metazoans caused by vital effects may not apply to microbialites. In microbial mats, several species of microbes are present and perhaps involved in the precipitation of microbial carbonates. In both of our modern samples, the most common microbes found in microbialites, cyanobacteria and sulfate-reducing bacteria, were likely present [24,76]. Despite the diversity of microbes within a microbial mat, Cr and $\delta^{53}\text{Cr}$ values in microbialites are homogeneous on the scale we investigated. This implies that the vital effects that seem to strongly affect the variability in $\delta^{53}\text{Cr}$ values in metazoans do not or insignificantly affect microbial carbonates.

On a cross-plot of Cr and $\delta^{53}\text{Cr}$ values, samples from both locations fell into site-specific groups with some overlap in their $\delta^{53}\text{Cr}$ values (Figure 5). This sharply contrasts the highly variable $\delta^{53}\text{Cr}$ values found in some metazoans. For example, different species of foraminifera from the West Pacific display $\delta^{53}\text{Cr}$ values between 0.21 and 2.37‰ [16]. The overlap in $\delta^{53}\text{Cr}$ values in stromatolite and tufa samples is remarkable, considering the differences in their formation, microbial community composition and morphology. For example, stromatolites in Marion Lake form from lithifying microbial mats, where organic substrates such as EPS are replaced by carbonates (e.g., [20,63]). In contrast, tufa in Mono Lake precipitates due to a combination of microbial activity and mixing of bicarbonate-rich lake

water with Ca-rich groundwater [37,49,50]. If these differences cause strong and distinct (vital) effects on Cr isotope fractionation, we would expect the two types of microbialites to have vastly different $\delta^{53}\text{Cr}$ values. Instead, despite these differences, their $\delta^{53}\text{Cr}$ values overlapped. This further confirms that Cr isotope fractionation is at least somewhat similar in the investigated types of microbialites. Thus, we found no evidence that differences in formation, microbial community composition and morphology of microbialites drive the variability of $\delta^{53}\text{Cr}$ values. We note that we did not investigate the microbial community compositions or structure and that our approach does not allow analysis of Cr isotope fractionation associated with specific bacterial metabolisms.

Although biological processes seem to have an insignificant effect on $\delta^{53}\text{Cr}$ variability, biological processes (e.g., metabolism of microbes) during incorporation of Cr into microbialites can still influence Cr isotope fractionation. Based on the knowledge on Cr isotope fractionation associated with organics, we propose a basic conceptual model for Cr incorporation and isotope fractionation in microbialites, assuming the presence of common cyanobacteria and sulfate-reducing bacteria. In this model (Figure 7; [55]), Cr(VI) from the fluid in which the microbial mat grows is partially reduced to Cr(III) by organic matter in a first step (1). This process was shown to favour isotopically light Cr (e.g., [6,15]). In organic-rich environments, such as within a microbial mat, the solubility of Cr(III) is increased due to complexation with ligands [77–79]. Thus, we suspect that (2) isotopically light Cr(III) is more likely to stay in solution compared with open marine conditions, (3) limiting its availability for precipitating carbonate. As a consequence, (4) isotopically heavy Cr(VI) is more efficiently incorporated into microbial carbonate (and associated organics) compared with skeletal carbonates precipitating under open marine conditions with high Cr(III) availability. The resulting $\delta^{53}\text{Cr}$ value in microbial carbonate is thus expected to show a smaller offset from ambient water compared with skeletal carbonates from open marine conditions. Furthermore, microbial carbonate is more likely to record a false positive, i.e., higher $\delta^{53}\text{Cr}$ values compared to ambient water than a false negative. This potentially also applies to ancient microbialites when extrapolating in the rock record.

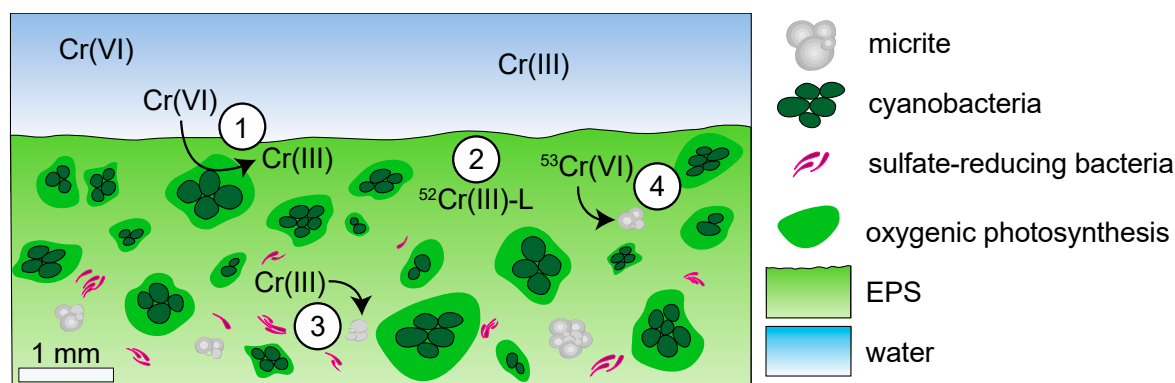


Figure 7. Illustration of a potential Cr incorporation pathway: (1) Cr reduction by microbes, (2) complexation of Cr(III) with ligands (L), which (3) limits its availability compared with open marine conditions. (4) Isotopically heavy Cr(VI) is incorporated into micritic carbonate. The general idea for carbonate precipitation within microbial mats is adapted from [80–82].

4.1.3. Environmental Controls on $\delta^{53}\text{Cr}$ Values in Modern Microbialites

There is a lack of evidence of biological controls causing Cr isotope variability in microbialites. Hence, we suspect that the differences in $\delta^{53}\text{Cr}$ values observed in microbialites from different locations are predominantly driven by environmental parameters. The main parameter influencing Cr isotope fractionation is redox state change since the reduction of Cr prefers isotopically light Cr (e.g., [3]). However, both of our modern microbialites formed in mostly oxygenated lakes and thus we cannot provide information on the influence of water column redox state on $\delta^{53}\text{Cr}$ values in microbialites. We note that the redox state within a microbial mat changes from oxic at the surface to anoxic with

depth, and this can affect $\delta^{53}\text{Cr}$ values. The $\delta^{53}\text{Cr}$ value in the oxic surface of the mat is likely equal to ambient water. However, at depth, where conditions within the mat are reducing, Cr reduction may cause lower $\delta^{53}\text{Cr}$ values than in the surface and thus a larger offset from the $\delta^{53}\text{Cr}$ value of ambient water. To decipher the effect of this redox-gradient on $\delta^{53}\text{Cr}$ value, investigations on a micro-scale are required.

Previous studies have shown that Cr isotope fractionation can be dependent on physico-chemical parameters. Here, we focused on pH and salinity [10,83], although other physico-chemical parameters may also be relevant. Laboratory experiments identified small $\Delta^{53}\text{Cr}$ values (0.06–0.29‰) in a pH range of ~8.5–10.4, and $\Delta^{53}\text{Cr} \approx 0\text{‰}$ for $\text{pH} \geq 9.4$ [9,10]. Two water bodies in the Southern Ocean with different salinities also show distinct $\delta^{53}\text{Cr}$ values, and their mixing leads to gradually changing $\delta^{53}\text{Cr}$ values [83]. Assuming $\Delta^{53}\text{Cr} \approx 0\text{‰}$ for Mono Lake ($\text{pH} \geq 9.2$ [46]), this agrees with [9,10]. However, also for Marion Lake, the estimated $\Delta^{53}\text{Cr}$ is $\approx 0\text{‰}$, whereas the pH range was lower (7.4–7.9; this study). Thus, our observations for natural samples only partially align with laboratory-precipitated carbonate, and pH does not seem to be the dominant influence on Cr isotope fractionation in these modern environments. Both our modern microbialites formed in hypersaline lakes (Marion Lake: >30 mg/L, Mono Lake: 90 g/L; [42,47], although salinity in Mono Lake was not constant over the last century [44]). It is thus possible that high salinity affected $\delta^{53}\text{Cr}$ values in our modern microbialites. Hypersaline conditions are conducive to microbial carbonate formation and can facilitate similar $\delta^{53}\text{Cr}$ and $\Delta^{53}\text{Cr}$ values at different sites. This supports our assumption that both $\Delta^{53}\text{Cr}$ values of Marion and Mono Lake microbialites are consistently small.

Stable C and O isotope ratios are commonly thought to reflect environmental conditions without being influenced by microbial metabolism [22,30,31]. Indeed, these data provide geochemical evidence that the modern microbialites were deposited in high-productive evaporative environments. The $\delta^{13}\text{C}$ values in Mono Lake microbialites reached values up to 8.52‰. Such high $\delta^{13}\text{C}$ values are typically observed in modern microbial carbonates, reflecting environments with extensive microbial activity. Further, high stable O isotope values of Marion Lake microbialites are indicative of an evaporative setting, such as a lagoon [84]. In contrast, $\delta^{18}\text{O}$ values of Mono Lake tufa can be attributed to geographic location and the influence of precipitation with depleted $\delta^{18}\text{O}$ values [84,85]. Since $\delta^{13}\text{C}$ and $\delta^{18}\text{O}$ values are known to record environmental conditions without being significantly influenced by microbial activity, the same may be true for $\delta^{53}\text{Cr}$ values. We acknowledge that these elements likely respond differently to both environmental and biological processes. However, due to the site-specific distinction in $\delta^{53}\text{Cr}$ values, stable C and O isotopes observed here, we propose that these geochemical tools are predominantly influenced by environmental rather than biological parameters.

The hypothesis that $\delta^{53}\text{Cr}$ values are mainly influenced by environmental conditions distinctive to marine vs. terrestrial settings (e.g., detrital contamination, pH, salinity) is further supported by REY data. Although REY abundance might be enriched during microbial stromatolite formation [65], patterns of REY in Marion and Mono Lake microbialites showed distinct differences that are consistent with their depositional environments [31,70]. Marion Lake microbialites formed in a coastal-influenced lake. Indeed, their typically marine REY patterns indicate that the influx of seawater strongly influences the water chemistry of Marion Lake microbialites (Figure 6). Samples from Mono Lake co-varied with the rather flat REY pattern of igneous rocks with overall high REY concentrations and a positive Eu anomaly that can also be representative of the hydrothermal environment in which these microbialites formed [86]. This pattern is consistent with the local water chemistry that is controlled by the surrounding mostly volcanic rocks (Figure 6; Table 4). The Ce anomaly in Mono Lake samples could indicate stratification of the water column or mixing of oxic lake water with anoxic ground water during tufa formation. The HREE of Mono Lake microbialites were slightly higher than LREE, in contrast with the basalt standard that shows a decrease in the concentrations of these elements. The slight enrichment in HREE in Mono Lake samples was consistent with previous observations in microbialites, where HREE can be complexed by organic components associated with microbialites (ligands, biofilms, EPS) and then preferentially incorporated, leading to an enrichment in HREE [70].

4.1.4. Comparison of Cr in Modern Microbialites and Seawater

The $\delta^{53}\text{Cr}$ values in our modern microbialite samples exhibit limited variation. For paleo-reconstructions, the $\delta^{53}\text{Cr}$ value within a water body is expected to be stable during the time relevant for microbialite growth. Hence, also the $\Delta^{53}\text{Cr}$ values ($\Delta^{53}\text{Cr}_{\text{microbialite-water}} = \delta^{53}\text{Cr}_{\text{microbialite}} - \delta^{53}\text{Cr}_{\text{water}}$) should not vary significantly. We estimated a $\delta^{53}\text{Cr}$ value of $\approx 1\text{‰}$ for Marion Lake water. This estimation is based on the $\delta^{53}\text{Cr}$ value of seawater from Lady Elliot Island, Australia ($0.72\text{--}1.01\text{‰}$; [17]), and average seawater $\delta^{53}\text{Cr}$ values ($0.41\text{--}1.72\text{‰}$; for references see [87]). Using this estimated $\delta^{53}\text{Cr}$ value, the $\Delta^{53}\text{Cr}$ value in Marion Lake is $\approx 0\text{‰}$, in line with previously reported values [17]. An estimation of a $\delta^{53}\text{Cr}$ value of Mono Lake water is challenging due to both the lack of Cr isotope data in lakes, as well as due to the complexity in evolution of Mono Lake. Anthropogenic influence led to substantial changes in the hydrology of Mono Lake (e.g., water level, concentration of solutes, mixing) [44]. Even though Mono Lake is surrounded by igneous rocks, which are known to carry $\delta^{53}\text{Cr}$ values of around -0.1‰ (e.g., [53,88]), the water $\delta^{53}\text{Cr}$ value can be well above the typical detrital Cr isotope composition (e.g., [89–91]). The range in $\delta^{53}\text{Cr}$ values of river waters draining igneous rock catchments is large ($-0.17\text{--}1.71\text{‰}$), but typically higher than 0.1‰ [89–91]. Thus, the $\delta^{53}\text{Cr}$ value of Mono Lake water is likely higher than 0.1‰ , and the offset between Mono Lake microbialites and ambient waters may approach a similarly small value as in Marion Lake ($\approx 0\text{‰}$). The estimated water $\delta^{53}\text{Cr}$ values are strongly simplified approximations and the Cr isotope offset between microbialites and water needs to be studied in detail.

The homogeneous $\delta^{53}\text{Cr}$ values in our microbialite samples likely also result in consistent Cr isotope offsets between microbialites and ambient waters. This opposes previous observations of biogenic carbonates, which are up to 0.9‰ lower than ambient water (corals and foraminifera; e.g., [13–19,75]). Incorporation of Cr into microbial carbonates seems to induce a consistent and potentially small fractionation effect contrasting the typical fractionation effects observed for metazoans (see Section 4.1.2). Hence, Cr isotope fractionation during incorporation in microbially-mediated carbonates perhaps more closely resembles the observations of abiotic experiments. Laboratory experiments precipitating inorganic calcite found small and positive $\Delta^{53}\text{Cr}$ values ($0.06\text{--}0.29\text{‰}$) for a pH range of $\sim 8.5\text{--}10.4$ [9], and $\Delta^{53}\text{Cr} \approx 0\text{‰}$ at pH > 9.4 [10]. Thus, for the Mono Lake site with a pH of ≥ 9.2 [46], a $\Delta^{53}\text{Cr}$ of $\approx 0\text{‰}$ is in line with the results from inorganically-precipitated calcite. Incorporation of Cr with isotope ratios similar to the ones in ambient waters due to a lack of vital effects enhances their reliability to reflecting $\delta^{53}\text{Cr}$ values of ambient waters with a consistent $\Delta^{53}\text{Cr}$ value. This is in agreement with [17] who suggested microbial carbonates as promising archives for paleo-reconstructions since these authors found $\delta^{53}\text{Cr}$ values in carbonates produced by a coralline red algae identical to ambient seawater.

4.2. Ancient Microbialites

4.2.1. Diagenetic Alteration of Ancient Microbialites

Chromium can be leached from carbonate sediments during diagenesis, leading to lower Cr and $\delta^{53}\text{Cr}$ values [54]. The ALG samples were dolomitized, but their textures and geochemistry show no severe alteration due to fluid mixing during burial [38]. Still, we cannot exclude that ancient $\delta^{53}\text{Cr}$ values are shifted towards lower values due to fluid mixing during burial [39]. Furthermore, our ancient samples showed slightly higher Cr compared with modern samples as well as a similarly small variability in $\delta^{53}\text{Cr}$ values (Figure 5). Thus, we infer that they were not significantly affected by Cr loss during diagenesis. However, we propose that the low Cr/Al ratio in the BSF samples indicates significant and potentially post-depositional alteration. This is also supported by BSF $\delta^{13}\text{C}$ and $\delta^{18}\text{O}$ values (Table 2). The BSF samples showed low $\delta^{13}\text{C}$ values paired with significantly lower $\delta^{18}\text{O}$ values, which points to a non-marine setting and perhaps a stronger degree of post-depositional diagenetic alteration compared to ALG samples. These samples should thus be considered unsuitable for paleo-environmental reconstructions using $\delta^{53}\text{Cr}$ as redox tracer.

4.2.2. Comparison of Modern and Ancient Microbialites

The differences in microbial community composition and structure between various modern, but also between modern and ancient microbialites can be substantial and potentially compromise comparability (reviewed by [92]). The two types of modern microbialites from marginal marine and non-marine environments we studied (stromatolite and tufa, respectively) provide insights into Cr isotope fractionation effects in these types of microbial carbonates. Like the modern samples, the $\delta^{53}\text{Cr}$ values that we measured in ancient microbialites from marginal marine (ALG) and evaporative lacustrine (BSF) environments were homogeneous and distinct (ALG: $0.36 \pm 0.14\text{‰}$, BSF: $-0.12 \pm 0.14\text{‰}$; Figures 3 and 5). These observations are first indicators that despite the diversity of microbialites in the present and through geological time scales, there are at least some similarities in their Cr isotope systematics. These similarities allow homogeneous incorporation of Cr from a presumably stable water column.

4.2.3. Biological and Environmental Controls on $\delta^{53}\text{Cr}$ Values in Ancient Microbialites

Assuming microbial activity does not significantly affect the behaviour of traditional geochemical tools recorded in microbialites, we propose that microbial activity did also not mask $\delta^{53}\text{Cr}$ values recorded by ancient microbialites, especially ALG samples. Although high $\delta^{13}\text{C}$ values of ALG samples ($+3.77 \pm 0.10\text{‰}$ (2SD); Figure 5; Table 2) can indicate environmental conditions with high microbial activity, they can also be indicative of an evaporative lagoon setting comparable to Marion Lake and the $\delta^{13}\text{C}$ data of modern Marion Lake microbialites. Thus, the $\delta^{53}\text{Cr}$ values of these samples are still thought to reflect environmental conditions. Further, due to presumably lower oxygen levels compared to present day, Cr(III) mobility was possibly increased relative to Cr(VI). As a result, more Cr(III) might have been incorporated in microbialites, leading to lower $\Delta^{53}\text{Cr}$ values. However, quantifying specific processes that may affect Cr isotope fractionation in the present or past exceeds the scope of this manuscript.

We propose that not only in the modern, but also in the ancient microbialites we investigated, the differences in $\delta^{53}\text{Cr}$ values were strongly affected by the depositional environment [1]. The non-marine samples (Mono Lake and BSF) showed higher Al concentrations compared to the marine samples. Mono Lake and BSF microbialites are surrounded by Al-rich volcanic rocks [44], and by silt- and mudstones [39], respectively. Both of these microbialites show low Cr/Al ratios, indicating that these samples were substantially influenced by detrital material. This is in agreement with the depositional environment, since these microbialites formed in an inland seaway or mud flat spreading over a metamorphic province. This is further supported by the flat REY pattern of the BSF samples, indicating detrital influence. The Eu anomaly was possibly caused by rivers draining igneous rocks and discharging in the lake in which the BSF microbialites precipitated (Figure 6). Contrasting these observations, no co-variations of $\text{Y}/\text{Ho}_{\text{SN}}$ and $\text{Eu}_{\text{SN}}/\text{Eu}^*_{\text{SN}}$ or $\text{Ce}_{\text{SN}}/\text{Ce}^*_{\text{SN}}$ were detected in BSF samples, indicating that detrital contamination was negligible. However, the preservation potential of marine REY patterns in Proterozoic carbonates is limited, for example due to overprinting with meteoric waters or REY-enriched particles [72].

Environmental parameters driving $\delta^{53}\text{Cr}$ values in microbialites include—besides depositional settings—salinity. The $\delta^{53}\text{Cr}$ values in microbialites from the marginal marine environment (ALG) are with $\approx 0.36\text{‰}$ higher compared with the ones from the evaporative lacustrine (BSF) setting ($\approx -0.12\text{‰}$), although BSF samples did not show pristine $\delta^{53}\text{Cr}$ values. While Marion Lake and ALG microbialites were deposited under marine-influenced conditions (higher $\delta^{53}\text{Cr}$ values than Mono Lake and BSF, respectively), both Mono Lake and our BSF samples are non-marine (lower $\delta^{53}\text{Cr}$ values than Marion Lake and ALG, respectively). Even though salinity may have some control on Cr isotope variability [83,93], all our samples were deposited under high-salinity conditions (hypersaline for Marion Lake, Mono Lake and BSF, and (evaporative) shallow-water conditions for ALG [38,39]). Thus, salinity is unlikely to explain the observed site-specific $\delta^{53}\text{Cr}$ values in our samples.

4.2.4. Comparison of Abiotic and Microbial Carbonates from the Precambrian

Our Cr data on ancient microbialites compare well with published data on Cr and Cr isotope compositions in Precambrian carbonates (Figure 5; e.g., [68]). Together with many Precambrian carbonate samples (e.g., [52,54], not illustrated in Figure 5), the BSF microbialites analysed in this study fell in the range of detrital $\delta^{53}\text{Cr}$ values. Typically, such low $\delta^{53}\text{Cr}$ values are attributed to the lack of atmospheric oxygen and immobility of poorly soluble Cr(III) (e.g., [1,52]). However, the BSF record comprises large magnitude $\delta^{13}\text{C}$ excursions, anhydrite-bearing red beds and evaporites, indicating the presence of a locally oxygenated atmosphere [39,94]. Since the presence of atmospheric oxygen induces Cr isotope fractionation, it is unlikely that the $\delta^{53}\text{Cr}$ value in the water from which BSF microbialites precipitated was unfractionated. Hence, in our BSF samples, detrital contamination and diagenesis masked the effect of atmospheric oxygen on Cr isotope fractionation.

In contrast, our ALG samples showed similar Cr and $\delta^{53}\text{Cr}$ values as some limestones and dolostone from the Yangtze Platform (Dengying Formation, 593 Ma; [68]) as well as from the Otavi Group (Namibia, ≈ 580 –770 Ma; [69]), Turukhansk Uplift (Siberia, ≈ 900 –1035 Ma), Angmaat Formation (Canada, ≈ 1092 Ma) and the Vazante Group (Brasil, ≈ 1112 Ma) [67]. While the carbonates underlying the Dengying Formation (Doushantuo Formation) have mostly negative $\delta^{53}\text{Cr}$ values [54,68], the Dengying Formation, as well as the ALG samples, showed $\delta^{53}\text{Cr}$ values above the detrital value (ALG: 0.23‰ or higher). Positively fractionated Cr isotope compositions back to approximately 1100 Ma are interpreted as indication of at least local oxygenation of oceans and atmosphere [1,55,68,69]). The shift to positive values is attributed to Cr isotope fractionation ultimately caused by oxygenation of the atmosphere (e.g., [2,52,95]). Under an at least locally oxygenated atmosphere, Cr(III) in terrestrial rocks is oxidised to Cr(VI) during weathering. Mobile Cr(VI) is transported to the oceans, where it can be reduced and thus fractionated. As a result, locally oxic water bodies carry isotopically heavier $\delta^{53}\text{Cr}$ values compared with anoxic oceans.

Importantly, the $\delta^{53}\text{Cr}$ values in our Proterozoic microbialites are in agreement with previously published data measured on carbonates, which supposedly were deposited abiotically. This finding supports our interpretation that environmental conditions are the main control on $\delta^{53}\text{Cr}$ values in microbialites. Detailed studies on, e.g., diagenetic alteration or dolomitization, are needed to reveal details on Cr isotope fractionation in microbial carbonates.

5. Implications and Conclusions

Despite the pervasive occurrence of microbialites in the Precambrian, the behaviour of Cr in microbially-precipitated carbonates has not yet been examined. We analyzed Cr and $\delta^{53}\text{Cr}$ values in modern and ancient microbialites from non-marine to marginal marine environments. Our data show homogeneous $\delta^{53}\text{Cr}$ values of sub-samples along profiles throughout all microbialites and site-specific $\delta^{53}\text{Cr}$ values. This observation is remarkable and promising, considering the diversity of microbial community compositions within a single microbialite. Overlapping $\delta^{53}\text{Cr}$ values in the two types of modern microbialites indicate that despite the differences in their formation and morphology, Cr isotope systematics seem to be similar. The lack of variability in $\delta^{53}\text{Cr}$ values due to biological parameters such as vital effects sharply contrasts the variability found in modern skeletal carbonates (such as mollusks or corals). The Cr and $\delta^{53}\text{Cr}$ values in our microbial carbonates from the Proterozoic are in good agreement with published Cr isotope data of presumably abiotic carbonates of similar age. This further supports our interpretation that variations in $\delta^{53}\text{Cr}$ values in microbial carbonates are driven by environmental rather than biological parameters. Due to the lack of evidence of biological processes driving $\delta^{53}\text{Cr}$ variability, we suggest that environmental parameters are the main control on Cr isotope variability in microbialites from different locations. Background lithology and salinity are among the environmental parameters that mostly affect Cr, but the specific processes are not fully resolved. Using stable C and O isotope compositions as well as REY patterns, we observed a strong influence of detrital contamination on Cr in microbialites that formed in environments where igneous rocks constitute the background lithology.

Environmental parameters can affect microbialite $\delta^{53}\text{Cr}$ data along with detrital contamination and (early) diagenetic alteration and have to be investigated in more detail. Still, our new results provide a promising foundation for the use of $\delta^{53}\text{Cr}$ values in microbialites for reconstructing the $\delta^{53}\text{Cr}$ values of the environments in which they formed.

Author Contributions: Conceptualization, S.B. and R.M.K.; methodology, S.B. and A.S.R.; formal analysis, S.B. and A.S.R.; investigation, S.B.; writing—original draft preparation, S.B., R.M.K., and A.S.R.; writing—review and editing, S.B., R.M.K., A.S.R., S.G., and R.F.; visualization, S.B.; supervision, S.G. and R.F.; project administration, S.G. and R.F.; funding acquisition, S.G. and R.F. All authors have read and agreed to the published version of the manuscript.

Funding: This research was funded by the European Union’s Horizon 2020 research and innovation program under the Marie Skłodowska-Curie grant agreement number 643084, and by the EOS-funded project *Evolution and Tracers of Habitability on Mars and the Earth* (ET-HOME).

Acknowledgments: We are grateful to V. Gostin (University of Adelaide) for providing microbialite samples from Marion Lake and Mono Lake. We thank T. Larsen for assistance in the laboratories and T. Leeper and T. Bech Ártung for support with mass spectrometry. We are particularly thankful to the National Parks and Wildlife Services, South Australia, for access to Marion Lake.

Conflicts of Interest: The authors declare no conflict of interest. The funders had no role in the design of the study; in the collection, analyses, or interpretation of data; in the writing of the manuscript, or in the decision to publish the results.

References

1. Gilleaudeau, G.J.; Voegelin, A.R.; Thibault, N.; Moreau, J.; Ullmann, C.V.; Klæbe, R.M.; Korte, C.; Frei, R. Stable isotope records across the Cretaceous–Paleogene transition, Stevns Klint, Denmark: New insights from the chromium isotope system. *Geochim. Cosmochim. Acta* **2018**, *235*, 305–332. [[CrossRef](#)]
2. Crowe, S.A.; Døssing, L.N.; Beukes, N.J.; Bau, M.; Kruger, S.J.; Frei, R.; Canfield, D.E. Atmospheric oxygenation three billion years ago. *Nature* **2013**, *501*, 535–538. [[CrossRef](#)]
3. Ellis, A.S.; Johnson, T.M.; Bullen, T.D. Chromium isotopes and the fate of hexavalent chromium in the environment. *Science* **2002**, *295*, 2060–2062. [[CrossRef](#)]
4. Schauble, E.; Rossman, G.R.; Taylor, H.P. Theoretical estimates of equilibrium chromium-isotope fractionations. *Chem. Geol.* **2004**, *205*, 99–114. [[CrossRef](#)]
5. Zink, S.; Schoenberg, R.; Staubwasser, M. Isotopic fractionation and reaction kinetics between Cr(III) and Cr(VI) in aqueous media. *Geochim. Cosmochim. Acta* **2010**, *74*, 5729–5745. [[CrossRef](#)]
6. Basu, A.; Johnson, T.M.; Sanford, R.A. Cr isotope fractionation factors for Cr(VI) reduction by a metabolically diverse group of bacteria. *Geochim. Cosmochim. Acta* **2014**, *142*, 349–361. [[CrossRef](#)]
7. Sikora, E.R.; Johnson, T.M.; Bullen, T.D. Microbial mass-dependent fractionation of chromium isotopes. *Geochim. Cosmochim. Acta* **2008**, *72*, 3631–3641. [[CrossRef](#)]
8. Tang, Y.; Elzinga, E.J.; Jae Lee, Y.; Reeder, R.J. Coprecipitation of chromate with calcite: Batch experiments and X-ray absorption spectroscopy. *Geochim. Cosmochim. Acta* **2007**, *71*, 1480–1493. [[CrossRef](#)]
9. Rodler, A.S.; Sánchez-Pastor, N.; Fernández-Díaz, L.; Frei, R. Fractionation behavior of chromium isotopes during coprecipitation with calcium carbonate: Implications for their use as paleoclimatic proxy. *Geochim. Cosmochim. Acta* **2015**, *164*, 221–235. [[CrossRef](#)]
10. Füger, A.; Bruggmann, S.; Frei, R.; Leis, A.; Dietzel, M.; Mavromatis, V. The role of pH on Cr(VI) partitioning and isotopic fractionation during its incorporation in calcite. *Geochim. Cosmochim. Acta* **2019**, *265*, 520–532. [[CrossRef](#)]
11. Saad, E.M.; Wang, X.; Planavsky, N.J.; Reinhard, C.T.; Tang, Y. Redox-independent chromium isotope fractionation induced by ligand-promoted dissolution. *Nat. Commun.* **2017**, *18*, 1–10. [[CrossRef](#)] [[PubMed](#)]
12. Kraemer, D.; Frei, R.; Viehmann, S.; Bau, M. Applied Geochemistry Mobilization and isotope fractionation of chromium during water-rock interaction in presence of siderophores. *Appl. Geochem.* **2019**, *102*, 44–54. [[CrossRef](#)]
13. Bonnand, P.; James, R.H.; Parkinson, I.J.; Connelly, D.P.; Fairchild, I.J. The chromium isotopic composition of seawater and marine carbonates. *Earth Planet. Sci. Lett.* **2013**, *382*, 528–535. [[CrossRef](#)]

14. Pereira, N.S.; Voegelin, A.R.; Paulukat, C.; Sial, A.N.; Ferreira, V.P.; Frei, R. Chromium-isotope signatures in scleractinian corals from the Rocas Atoll, Tropical South Atlantic. *Geobiology* **2015**, *1*, 1–14. [[CrossRef](#)] [[PubMed](#)]
15. Holmden, C.; Jacobson, A.D.; Sageman, B.B.; Hurtgen, M.T. Response of the Cr isotope proxy to Cretaceous Ocean Anoxic Event 2 in a pelagic carbonate succession from the Western Interior Seaway. *Geochim. Cosmochim. Acta* **2016**, *186*, 277–295. [[CrossRef](#)]
16. Wang, X.; Planavsky, N.J.; Hull, P.M.; Tripathi, A.E.; Zou, H.J.; Elder, L.; Henehan, M. Chromium isotopic composition of core-top planktonic foraminifera. *Geobiology* **2016**, *1*, 1–14. [[CrossRef](#)]
17. Farkaš, J.; Frýda, J.; Paulukat, C.; Hathorne, E.C.; Matoušková, Š.; Rohovec, J.; Frýdová, B.; Francová, M.; Frei, R. Chromium isotope fractionation between modern seawater and biogenic carbonates from the Great Barrier Reef, Australia: Implications for the paleo-seawater $\delta^{53}\text{Cr}$ reconstruction. *Earth Planet. Sci. Lett.* **2018**, *498*, 140–151. [[CrossRef](#)]
18. Frei, R.; Paulukat, C.; Bruggmann, S.; Kläbe, R.M. A systematic look at chromium isotopes in modern shells—Implications for paleo-environmental reconstructions. *Biogeosciences* **2018**, *15*, 4905–4922. [[CrossRef](#)]
19. Bruggmann, S.; Kläbe, R.M.; Paulukat, C.; Frei, R. Heterogeneity and incorporation of chromium isotopes in recent marine molluscs (*Mytilus*). *Geobiology* **2019**, *1*, 1–19. [[CrossRef](#)]
20. Burne, R.V.; Moore, L.S. Microbialites: Organosedimentary deposits of benthic microbial communities. *Soc. Sediment. Geol.* **1987**, *2*, 241–254. [[CrossRef](#)]
21. Reid, R.P.; Visscher, P.T.; Decho, A.W.; Stolz, J.F.; Bebout, B.M.; Dupraz, C.; Macintyre, I.G.; Paerl, H.W.; Pinckney, J.L.; Prufert-Bebout, L.; et al. The role of microbes in accretion, lamination and early lithification of modern marine stromatolites. *Nature* **2000**, *406*, 989–992. [[CrossRef](#)] [[PubMed](#)]
22. Grotzinger, J.P.; Knoll, A.H. Stromatolites in Precambrian carbonates: Evolutionary mileposts or environmental dipsticks? *Annu. Rev. Earth Planet. Sci.* **1999**, *27*, 313–358. [[CrossRef](#)] [[PubMed](#)]
23. Vasconcelos, C.; Warthmann, R.; McKenzie, J.A.; Visscher, P.T.; Bittermann, A.G.; van Lith, Y. Lithifying microbial mats in Lagoa Vermelha, Brazil: Modern Precambrian relics? *Sediment. Geol.* **2006**, *185*, 175–183. [[CrossRef](#)]
24. Perri, E.; Tucker, M.E.; Spadafora, A.; Università, T. Carbonate organo-mineral micro- and ultrastructures in sub-fossil stromatolites: Marion lake, South Australia. *Geobiology* **2012**, *10*, 105–117. [[CrossRef](#)]
25. Ueno, Y.; Isozaki, Y.; Yurimoto, H.; Maruyama, S. Carbon isotopic signatures of individual Archean microfossils (?) from Western Australia. *Int. Geol. Rev.* **2001**, *43*, 196–212. [[CrossRef](#)]
26. Ueno, Y.; Maruyama, S.; Isozaki, Y. Early Archean (ca. 3.5 Ga) microfossils and ^{13}C -depleted carbonaceous matter in the North Pole area, Western Australia: Field occurrence and geochemistry. In *Geochemistry and the Origin of Life*; Nakasima, S., Maruyama, S., Brack, A., Windley, B.F., Eds.; Universal Academic Press: New York, NY, USA, 2001; pp. 203–236.
27. van Kranendonk, M.J.; Webb, G.E.; Kamber, B.S. Geological and trace element evidence for a marine sedimentary environment of deposition and biogenicity of 3.45 Ga stromatolitic carbonates in the Pilbara Craton, and support for a reducing Archaean ocean. *Geobiology* **2003**, *1*, 91–108. [[CrossRef](#)]
28. Allwood, A.C.; Kamber, B.S.; Walter, M.R.; Burch, I.W.; Kanik, I. Trace elements record depositional history of an Early Archean stromatolitic carbonate platform. *Chem. Geol.* **2010**, *270*, 148–163. [[CrossRef](#)]
29. Nutman, A.P.; Bennett, V.C.; Friend, C.R.L.; Van Kranendonk, M.J.; Chivas, A.R. Rapid emergence of life shown by discovery of 3700-million-year-old microbial structures. *Nature* **2016**, *537*, 535–538. [[CrossRef](#)]
30. Riding, R. Microbial carbonates: The geological record of calcified bacterial-algal mats and biofilms. *Sedimentology* **2000**, *47*, 179–214. [[CrossRef](#)]
31. Webb, G.E.; Kamber, B.S. Rare earth elements in Holocene reefal microbialites: A new shallow seawater proxy. *Geochim. Cosmochim. Acta* **2000**, *64*, 1–9. [[CrossRef](#)]
32. Johannesson, K.H.; Hawkins, D.L.; Cortés, A. Do Archean chemical sediments record ancient seawater rare earth element patterns? *Geochim. Cosmochim. Acta* **2006**, *70*, 871–890. [[CrossRef](#)]
33. Elderfield, H.; Upstill-Goddard, R.; Sholkovitz, E.R. The rare earth elements in rivers, estuaries, and coastal seas and their significance to the composition of ocean waters. *Geochim. Cosmochim. Acta* **1990**, *54*, 971–991. [[CrossRef](#)]

34. Planavsky, N.; Bekker, A.; Rouxel, O.J.; Kamber, B.; Hofmann, A.; Knudsen, A.; Lyons, T.W. Rare Earth Element and yttrium compositions of Archean and Paleoproterozoic Fe formations revisited: New perspectives on the significance and mechanisms of deposition. *Geochim. Cosmochim. Acta* **2010**, *74*, 6387–6405. [[CrossRef](#)]
35. Bau, M.; Möller, P. Rare earth element systematics of the chemically precipitated component in early precambrian iron formations and the evolution of the terrestrial atmosphere-hydrosphere-lithosphere system. *Geochim. Cosmochim. Acta* **1993**, *57*, 2239–2249. [[CrossRef](#)]
36. Nothdurft, L.D.; Webb, G.E.; Kamber, B.S. Rare earth element geochemistry of Late Devonian reefal carbonates, Canning Basin, Western Australia: Confirmation of a seawater REE proxy in ancient limestones. *Geochim. Cosmochim. Acta* **2004**, *68*, 263–283. [[CrossRef](#)]
37. Whiticar, M.J.; Suess, E. The cold carbonate connection between Mono Lake, California and the Bransfield Strait, Antarctica. *Aquat. Geochem.* **1998**, *4*, 429–454. [[CrossRef](#)]
38. Klæbe, R.M.; Smith, M.P.; Fairchild, I.J.; Fleming, E.J.; Kennedy, M.J. Facies-dependent $\delta^{13}\text{C}$ variation and diagenetic overprinting at the onset of the Sturtian glaciation in North-East Greenland. *Precambrian Res.* **2018**, *319*, 96–113. [[CrossRef](#)]
39. Klæbe, R.M.; Kennedy, M.J.; Jarrett, A.J.M.; Brocks, J.J. Local paleoenvironmental controls on the carbon-isotope record defining the Bitter Springs Anomaly. *Geobiology* **2016**, *15*, 65–80. [[CrossRef](#)]
40. von der Borch, C.C.; Bolton, B.; Warren, J.K. Environmental setting and microstructure of subfossil lithified stromatolites associated with evaporites. *Sedimentology* **1977**, *24*, 693–708. [[CrossRef](#)]
41. Warren, J.K. The Hydrological Significance of Holocene Tepees, Stromatolites, and Boxwork Limestones in Coastal Salinas in South Australia. *J. Sediment. Res.* **1982**, *52*, 1171–1201.
42. Pilkington, G. *Resistivity Survey near Stenhouse Bay, Yorke Peninsula*; South Australian Department of Mines and Energy: Adelaide, SA, Australia, 1977; Unpublished work.
43. Warren, J.K. The hydrological setting, occurrence and significance of gypsum in late Quaternary salt lakes in South Australia. *Sedimentology* **1982**, *29*, 603–637. [[CrossRef](#)]
44. Johannesson, K.H.; Lyons, W.B. The rare earth element geochemistry of Mono Lake water and the importance of carbonate complexing. *Limnol. Oceanogr.* **1994**, *39*, 1141–1154. [[CrossRef](#)]
45. Oremland, R.S.; Stolz, J.F.; Hollibaugh, J.T. The microbial arsenic cycle in Mono Lake, California. *Fems Microb. Ecol.* **2004**, *48*, 15–27. [[CrossRef](#)] [[PubMed](#)]
46. Stam, M.C.; Mason, P.R.D.; Pallud, C.; Van Cappellen, P. Sulfate reducing activity and sulfur isotope fractionation by natural microbial communities in sediments of a hypersaline soda lake (Mono Lake, California). *Chem. Geol.* **2010**, *278*, 23–30. [[CrossRef](#)]
47. Herbst, D.B. Potential salinity limitations on nitrogen fixation in sediments from Mono Lake, California. *Int. J. Salt Lake Res.* **1998**, *7*, 261–274. [[CrossRef](#)]
48. Domagalski, J.L.; Eugster, H.P.; Jones, B.F. Trace metal geochemistry of Walker, Mono, and Great Salt Lakes. In *Fluid-Mineral Interactions: A Tribute to H.P. Eugster*; Spencer, R.J., Chou, I.M., Eds.; The Geochemical Society: Pergamon, Turkey, 1990; pp. 315–353.
49. Scholl, D.W.; Taft, W.H. Algae, contributors to the formation of calcareous tufa, Mono Lake, California. *J. Sediment. Petrol.* **1964**, *34*, 309–319.
50. Pedley, M.; Rogerson, M.; Middleton, R. Freshwater calcite precipitates from in vitro mesocosm flume experiments: A case for biomediation of tufas. *Sedimentology* **2009**, *56*, 511–527. [[CrossRef](#)]
51. Brasier, A.; Wacey, D.; Rogerson, M.; Guagliardo, P.; Saunders, M.; Kellner, S.; Mercedes-Martin, R.; Prior, T.; Taylor, C.; Matthews, A.; et al. A microbial role in the construction of Mono Lake carbonate chimneys? *Geobiology* **2018**, *16*, 540–555. [[CrossRef](#)] [[PubMed](#)]
52. Frei, R.; Gaucher, C.; Døssing, L.N.; Sial, A.N. Chromium isotopes in carbonates - A tracer for climate change and for reconstructing the redox state of ancient seawater. *Earth Planet. Sci. Lett.* **2011**, *312*, 114–125. [[CrossRef](#)]
53. Schoenberg, R.; Zink, S.; Staubwasser, M.; Blanckenburg, F. Von The stable Cr isotope inventory of solid Earth reservoirs determined by double spike MC-ICP-MS. *Chem. Geol.* **2008**, *249*, 294–306. [[CrossRef](#)]
54. Rodler, A.S.; Hohl, S.V.; Guo, Q.; Frei, R. Chromium isotope stratigraphy of Ediacaran cap dolostones, Doushantuo. *Chem. Geol.* **2016**, *436*, 24–34. [[CrossRef](#)]

55. Rodler, A.S.; Frei, R.; Gaucher, C.; Korte, C.; Rosing, S.A.; Germs, G.J.B. Multiproxy isotope constraints on ocean compositional changes across the late Neoproterozoic Ghaub glaciation, Otavi Group, Namibia. *Precambrian Res.* **2017**, *298*, 306–324. [[CrossRef](#)]
56. D'Arcy, J.; Gilleaudeau, G.; Peralta, S.; Frei, R. Redox fluctuations in the Early Ordovician oceans: An insight from chromium stable isotopes. *Chem. Geol.* **2017**, *448*, 1–12. [[CrossRef](#)]
57. Imai, A.; Gloyna, E.F. Effects of pH and oxidation state of chromium on the behavior of chromium in the activated sludge process. *Water Res.* **1990**, *24*, 1143–1150. [[CrossRef](#)]
58. Bonnand, P.; Parkinson, I.J.; James, R.H.; Karjalainen, A.; Fehr, M.A. Accurate and precise determination of stable Cr isotope compositions in carbonates by double spike MC-ICP-MS. *J. Anal. At. Spectrom.* **2011**, *26*, 528. [[CrossRef](#)]
59. Planavsky, N.J.; Reinhard, C.T.; Wang, X.; Thomson, D.; Mcgoldrick, P.; Rainbird, R.H.; Johnson, T.; Fischer, W.W.; Lyons, T.W. Low Mid-Proterozoic atmospheric oxygen levels and the delayed rise of animals. *Science* **2014**, *346*, 635–638. [[CrossRef](#)]
60. Taylor, S.R.; McLennan, S.M. *The Continental Crust: Its Composition and Evolution*; Blackwell: Hoboken, NJ, USA, 1985.
61. Nance, W.B.; Taylor, S.R. Rare earth element patterns and crustal sedimentary rocks. *Geochim. Cosmochim. Acta* **1976**, *40*, 1539–1551. [[CrossRef](#)]
62. Bau, M.; Dulski, P. Distribution of yttrium and rare-earth elements in the Penge and Kuruman iron-formations, Transvaal Supergroup, South Africa. *Precambrian Res.* **1996**, *79*, 37–55. [[CrossRef](#)]
63. Bolhar, R.; Kamber, B.S.; Moorbath, S.; Fedo, C.M.; Whitehouse, M.J. Characterisation of early Archaean chemical sediments by trace element signatures. *Earth Planet. Sci. Lett.* **2004**, *222*, 43–60. [[CrossRef](#)]
64. Bau, M.; Dulski, P. Comparing yttrium and rare earths in hydrothermal fluids from the Mid-Atlantic Ridge: Implications for Y and REE behaviour during near-vent mixing and for the Y/Ho ratio of Proterozoic seawater. *Chem. Geol.* **1999**, *155*, 77–90353. [[CrossRef](#)]
65. Viehmann, S.; Hohl, S.V.; Kraemer, D.; Bau, M.; Walde, D.H.G.; Galer, S.J.G.; Jiang, S.; Meister, P. Metal cycling in Mesoproterozoic microbial habitats: Insights from trace elements and stable Cd isotopes in stromatolites. *Gondwana Res.* **2019**, *67*, 101–114. [[CrossRef](#)]
66. Lawrence, M.G.; Kamber, B.S. The behaviour of the rare earth elements during estuarine mixing—Revisited. *Mar. Chem.* **2006**, *100*, 147–161. [[CrossRef](#)]
67. Gilleaudeau, G.J.; Frei, R.; Kaufman, A.J.; Kah, L.C.; Azmy, K.; Bartley, J.K.; Chernyavskiy, P.; Knoll, A.H. Oxygenation of the mid-Proterozoic atmosphere: Clues from chromium isotopes in carbonates. *Geochem. Perspect. Lett.* **2016**, *2*, 178–187. [[CrossRef](#)]
68. Wei, W.; Frei, R.; Gilleaudeau, J.; Li, D.; Wei, G.; Chen, X. Oxygenation variations in the atmosphere and shallow seawaters of the Yangtze Platform during the Ediacaran Period: Clues from Cr-isotope and Ce-anomaly in carbonates. *Precambrian Res.* **2018**, *313*, 78–90. [[CrossRef](#)]
69. Rodler, A.S.; Frei, R.; Gaucher, C.; Germs, G.J.B. Chromium isotope, REE and redox-sensitive trace element chemostratigraphy across the late Neoproterozoic Ghaub glaciation, Otavi Group, Namibia. *Precambrian Res.* **2016**, *286*, 234–249. [[CrossRef](#)]
70. Johannesson, K.H.; Telfeyan, K.; Chevis, D.A.; Rosenheim, B.E.; Leybourne, M.L. Rare earth elements in stromatolites—1. Evidence that modern terrestrial stromatolites fractionate rare earth elements during incorporation from ambient waters. In *Evolution of Archean Crust and Early Life*; Springer: Dordrecht, The Netherlands; Berlin/Heidelberg, Germany, 2014; pp. 385–411.
71. van de Flierdt, T.; Pahnke, K.; Basak, C.; Coles, B.; Colin, C.; Crocket, K.; Frank, M.; Frank, N.; Goldstein, S.L.; Goswami, V.; et al. GEOTRACES intercalibration of neodymium isotopes and rare earth element concentrations in seawater and suspended particles. Part 1: Reproducibility of results for the international intercomparison. *Limnol. Oceanogr. Methods* **2012**, *234*–251. [[CrossRef](#)]
72. Frimmel, H.E. Trace element distribution in Neoproterozoic carbonates as palaeoenvironmental indicator. *Chem. Geol.* **2009**, *258*, 338–353. [[CrossRef](#)]
73. Sforza, M.C.; Daye, M.; Philippot, P.; Somogyi, A.; van Zuilen, M.A.; Medjoubi, K.; Gérard, E.; Jamme, F.; Dupraz, C.; Braissant, O.; et al. Patterns of metal distribution in hypersaline microbialites during early diagenesis: Implications for the fossil record. *Geobiology* **2017**, *15*, 259–279. [[CrossRef](#)]

74. Valdespino-Castillo, P.M.; Hu, P.; Merino-Ibarra, M.; López-Gómez, L.M.; Cerqueda-García, D.; González-De Zayas, R.; Pi-Puig, T.; Lestayo, J.A.; Holman, H.Y.; Falcón, L.I. Exploring biogeochemistry and microbial diversity of extant microbialites in Mexico and Cuba. *Front. Microbiol.* **2018**, *9*, 1–22. [\[CrossRef\]](#) [\[PubMed\]](#)
75. Remmelzwaal, S.R.C.; Yu, A.; Parkinson, I.J.; Schmidt, D.N.; Titelboim, D.; Abramovich, S.; Roepert, A.; Kienhuis, M.; Polerecky, L.; Goring-harford, H.; et al. Post-depositional overprinting of chromium in foraminifera. *Earth Planet. Sci. Lett.* **2019**, *515*, 100–111. [\[CrossRef\]](#)
76. Souza-Egipsy, V.; Wierzbos, J.; Ascaso, C.; Nealson, K.H. Mg–silica precipitation in fossilization mechanisms of sand tufa endolithic microbial community, Mono Lake (California). *Chem. Geol.* **2005**, *217*, 77–87. [\[CrossRef\]](#)
77. Connelly, D.P.; Statham, P.J.; Knap, A.H. Seasonal changes in speciation of dissolved chromium in the surface Sargasso Sea. *Deep-Sea Res. I* **2006**, *53*, 1975–1988. [\[CrossRef\]](#)
78. Sander, S.; Koschinsky, A. Onboard-ship redox speciation of chromium in diffuse hydrothermal fluids from the North Fiji Basin. *Mar. Chem.* **2000**, *71*, 83–102. [\[CrossRef\]](#)
79. Sander, S.; Koschinsky, A. Metal flux from hydrothermal vents increased by organic complexation. *Nat. Publ. Group* **2011**, *4*, 145–150. [\[CrossRef\]](#)
80. Spadafora, A.; Perri, E.; Mckenzie, J.A.; Vasconcelos, C. Microbial biomineralization processes forming modern Ca:Mg carbonate stromatolites. *Sedimentology* **2010**, *57*, 27–40. [\[CrossRef\]](#)
81. Pace, A.; Bourillot, R.; Bouton, A.; Vennin, E.; Galaup, S.; Bundeleva, I.; Patrier, P.; Dupraz, C.; Thomazo, C.; Sansjofre, P.; et al. Microbial and diagenetic steps leading to the mineralisation of Great Salt Lake microbialites. *Nat. Publ. Group* **2016**, 1–12. [\[CrossRef\]](#) [\[PubMed\]](#)
82. Pace, A.; Bourillot, R.; Bouton, A.; Vennin, E.; Braissant, O.; Dupraz, C.; Duteil, T.; Bundeleva, I.; Patrier, P.; Galaup, S.; et al. Formation of stromatolite lamina at the interface of oxygenic-anoxigenic photosynthesis. *Geobiology* **2018**, 1–21. [\[CrossRef\]](#) [\[PubMed\]](#)
83. Rickli, J.; Janssen, D.J.; Hassler, C.; Ellwood, M.J.; Jaccard, S.L. Chromium biogeochemistry and stable isotope distribution in the Southern Ocean. *Geochim. Cosmochim. Acta* **2019**, *262*, 188–206. [\[CrossRef\]](#)
84. Talbot, M.R. A review of the palaeohydrological interpretation of carbon and oxygen isotopic ratios in primary lacustrine carbonates. *Chem. Geol.* **1990**, *80*, 261–279. [\[CrossRef\]](#)
85. Li, H.; Ku, T.; Stott, L.D.; Anderson, R.F. Stable isotope studies on Mono Lake (California). 1. $\delta^{18}O$ in lake sediments as proxy for climatic change during the last 150 years Mono Lake hydrology. *Limnol. Oceanogr.* **1997**, *42*, 230–238. [\[CrossRef\]](#)
86. Meyer, E.E.; Quicksall, A.N.; Landis, J.D.; Link, P.K.; Bostick, B.C. Trace and rare earth elemental investigation of a Sturtian cap carbonate, Pocatello, Idaho: Evidence for ocean redox conditions before and during carbonate deposition. *Precambrian Res.* **2012**, *192–195*, 89–106. [\[CrossRef\]](#)
87. Nasemann, P.; Janssen, D.J.; Rickli, J.; Grasse, P.; Frank, M.; Jaccard, S.L. Chromium reduction and associated stable isotope fractionation restricted to anoxic shelf waters in the Peruvian Oxygen Minimum Zone. *Geochim. Cosmochim. Acta* **2020**, *285*, 207–224. [\[CrossRef\]](#)
88. Farkaš, J.; Chrástny, V.; Novák, M.; Cadkova, E.; Pasava, J.; Chakrabarti, R.; Jacobsen, S.B.; Ackermann, L.; Bullen, T.D. Chromium isotope variations ($\delta^{53}/^{52}Cr$) in mantle-derived sources and their weathering products: Implications for environmental studies and the evolution of $\delta^{53}/^{52}Cr$ in the Earth's mantle over geologic time. *Geochim. Cosmochim. Acta* **2013**, *123*, 74–92. [\[CrossRef\]](#)
89. D'Arcy, J.D.; Babechuk, M.G.; Nørbye, L.; Gaucher, C.; Frei, R. Processes controlling the chromium isotopic composition of river water: Constraints from basaltic river catchments. *Geochim. Cosmochim. Acta* **2016**, *186*, 296–315. [\[CrossRef\]](#)
90. Sun, Z.; Wang, X.; Planavsky, N. Cr isotope systematics in the Connecticut River estuary. *Chem. Geol.* **2019**, *506*, 29–39. [\[CrossRef\]](#)
91. Wu, W.; Wang, X.; Reinhard, C.T.; Planavsky, N.J. Chromium isotope systematics in the Connecticut River. *Chem. Geol.* **2017**, *456*, 98–111. [\[CrossRef\]](#)
92. Cantine, M.D.; Knoll, A.H.; Bergmann, K.D. Carbonates before skeletons: A database approach. *Earth-Sci. Rev.* **2020**, *201*. [\[CrossRef\]](#)
93. Scheiderich, K.; Amini, M.; Holmden, C.; Francois, R. Global variability of chromium isotopes in seawater demonstrated by Pacific, Atlantic, and Arctic Ocean samples. *Earth Planet. Sci. Lett.* **2015**, *423*, 87–97. [\[CrossRef\]](#)

94. Fike, D.A.; Grotzinger, J.P.; Pratt, L.M.; Summons, R.E. Oxidation of the Ediacaran Ocean. *Nature* **2006**, *444*, 744–747. [[CrossRef](#)]
95. Frei, R.; Gaucher, C.; Poulton, S.W.; Canfield, D.E. Fluctuations in Precambrian atmospheric oxygenation recorded by chromium isotopes. *Nature* **2009**, *461*, 250–253. [[CrossRef](#)]

Publisher’s Note: MDPI stays neutral with regard to jurisdictional claims in published maps and institutional affiliations.



© 2020 by the authors. Licensee MDPI, Basel, Switzerland. This article is an open access article distributed under the terms and conditions of the Creative Commons Attribution (CC BY) license (<http://creativecommons.org/licenses/by/4.0/>).